

Salinity Trends within the Upper Layers of the Subpolar North Atlantic

JAN-ERIK TESDAL, RYAN P. ABERNATHEY, JOAQUIM I. GOES, AND ARNOLD L. GORDON

Lamont-Doherty Earth Observatory, Columbia University, Palisades, New York

THOMAS W. N. HAINE

Department of Earth and Planetary Sciences, The Johns Hopkins University, Baltimore, Maryland

(Manuscript received 9 August 2017, in final form 21 November 2017)

ABSTRACT

Examination of a range of salinity products collectively suggests widespread freshening of the North Atlantic from the mid-2000s to the present. Monthly salinity fields reveal negative trends that differ in magnitude and significance between western and eastern regions of the North Atlantic. These differences can be attributed to the large negative interannual excursions in salinity in the western subpolar gyre and the Labrador Sea, which are not apparent in the central or eastern subpolar gyre. This study demonstrates that temporal trends in salinity in the northwest (including the Labrador Sea) are subject to mechanisms that are distinct from those responsible for the salinity trends in the central and eastern North Atlantic. In the western subpolar gyre a negative correlation between near-surface salinity and the circulation strength of the subpolar gyre suggests that negative salinity anomalies are connected to an intensification of the subpolar gyre, which is causing increased flux of freshwater from the East Greenland Current and subsequent transport into the Labrador Sea during the melting season. Analyses of sea surface wind fields suggest that the strength of the subpolar gyre is linked to the North Atlantic Oscillation– and Arctic Oscillation–driven changes in wind stress curl in the eastern subpolar gyre. If this trend of decreasing salinity continues, it has the potential to enhance water column stratification, reduce vertical fluxes of nutrients, and cause a decline in biological production and carbon export in the North Atlantic Ocean.

1. Introduction

Changes in salinity affect buoyancy and density stratification in the northern North Atlantic, and numerous studies have exemplified the implications of this process for deep convection in the Labrador Sea (Gelderloos et al. 2012; Böning et al. 2016; Yang et al. 2016), Irmingier Sea (Våge et al. 2011), and Greenland Sea (Marshall and Schott 1999). Therefore, variability in salinity plays an important role in meridional overturning circulation and the global climate (Buckley and Marshall 2016). It has also been shown that variations in salinity are a key to the amount of heat that can be taken up by the deep ocean of the North Atlantic. As described by Mauritzen et al. (2012), higher salinity allows density-compensated heat uptake to occur, in which warmer water masses are able to sink into the deep ocean, leading to greater ocean heat uptake. By altering

the timing, magnitude, and spatial distribution of water-column stratification, changes to salinity can also affect the overall abundance and seasonal blooming of phytoplankton, zooplankton, and consumers on higher trophic levels (Greene et al. 2012; Li et al. 2015). Thus, changes in salinity can have substantial implications in a wide range of processes in the North Atlantic.

Since the 1960s, several studies have noted stark shifts in salinity in the subpolar North Atlantic (Dickson et al. 1988; Curry et al. 2003; Curry and Mauritzen 2005; Boyer et al. 2007). In recent years, a persistent imbalance of sea ice melting versus sea ice growth (Comiso et al. 2008; Parkinson and Comiso 2013), changes in Arctic and North American river discharge (Peterson et al. 2002, 2006; Déry et al. 2009; Dyrgerov et al. 2010), an intensification of the hydrological cycle (i.e., increased net precipitation vs evaporation) (Kattsov and Walsh 2000; Durack et al. 2012), and glacial melt anomalies such as the Greenland ice melt (Bamber et al. 2012; Yang et al. 2016) have been observed. This raises the intriguing possibility of an enduring decline in sea surface salinity in

Corresponding author: Jan-Erik Tesdal, tesdal@ldeo.columbia.edu

the Arctic and subpolar North Atlantic and more dramatic shifts in salinity in coming years.

It is becoming increasingly evident that, since the mid-1990s, salinity in the Arctic Ocean has been on a decline, as seen by an increase in the Arctic freshwater content (Proshutinsky et al. 2009). Rabe et al. (2014) estimated this increase in liquid freshwater content to be around $600 \pm 300 \text{ km}^3 \text{ yr}^{-1}$ in the upper Arctic Ocean from 1992 to 2012. Since a major fraction of the Arctic waters outflow into the North Atlantic, it is expected that an increase in the freshwater content in the Arctic would result in an increase in the freshwater content in the North Atlantic as well. However, recent studies have shown that increased freshening in the Arctic has an anticorrelation with salinity trends in the North Atlantic and that freshwater release from the Arctic may occur on a decadal time scale in response to large-scale changes in atmospheric variability (Stewart and Haine 2013). These findings imply that declining salinity in the Arctic may not be the immediate driving factor for current trends in the North Atlantic. However, further, and much more dramatic, decreases in salinity may occur in the North Atlantic in response to the long-term effects of North Atlantic–Arctic exchanges occurring over decadal time scales.

Changes in the freshwater content in the North Atlantic have been investigated in a number of studies (e.g., Dickson et al. 2002; Curry and Mauritzen 2005; Boyer et al. 2007). None of these studies have revealed a consistent decline in salinity over the past decades. Instead there have been discrete events as documented by Dickson et al. (1988), Belkin et al. (1998), and Belkin (2004) where unusual freshening of the North Atlantic, known as Great Salinity Anomalies (GSAs), have occurred. GSAs are mostly associated with increased freshwater outflow from the Arctic. However, other processes often play an important role in their formation. The GSA in the 1980s is believed to have been primarily formed within the Labrador Sea and Baffin Bay regions (Belkin et al. 1998), while the GSA in the 1990s has been partly associated with reduced northward transport of higher-salinity waters (Häkkinen 2002). Explorations of salinity trends for the recent time period using Argo floats have shown a general decreasing trend in high latitudes and an increase in surface salinity in the lower latitudes (Johnson and Lyman 2016). These regional trends have been attributed to an acceleration of the hydrological cycle, wherein decreasing salinity trends in high latitudes are influenced by an overall increase in precipitation, and increasing salinity trends in lower latitudes are influenced by an overall increase in evaporation (Durack et al. 2012).

In this study, gridded monthly mean temperature and salinity ($T-S$) fields from a variety of objective analysis (OA) and reanalysis data products are used in order to better understand the recent trends in salinity in the North Atlantic Ocean and the underlying causes for the changes observed. For the OA products, the monthly fields have been derived from available hydrographic data. There is considerable overlap in terms of the in situ data that has gone into these datasets, but most of it comes from the Argo float program. Argo floats, which began operation in the early 2000s, have dramatically improved the spatial and temporal coverage of temperature and salinity in much of the upper 2000 m of the global ice-free oceans, offsetting some of the regional and seasonal biases inherent in previous, solely shipboard observation-based gridded datasets (Riser et al. 2016).

The Argo observation system, which now maintains almost 4000 well-distributed floats on a global scale, has made possible the production of a number of OA $T-S$ fields based exclusively on in situ data. Coverage is still limited in regions where the sea floor is too shallow (e.g., near the coasts) or where the surface is often obstructed by sea ice (e.g., Arctic Ocean), but the number of Argo floats continues to expand, and new float types are being developed to provide observations in regions that are still underrepresented. For the central Arctic ice zones ice-tethered profilers (ITPs) provide high-resolution vertical profiles similar to those obtained by Argo floats (Toole et al. 2011). However, ITPs do not extend to the adjacent seas, such as Baffin Bay, the Labrador Sea, or the Greenland Sea.

There have been no detailed investigations into the recent trends in the North Atlantic, for which much better coverage exists owing to Argo data collection. This study presents a comparison of trends in near-surface salinity among available data products. The comparison identifies regions where datasets show similar patterns, as well as regions where datasets disagree, for the time period when Argo salinity measurements exist (2000–15). Trends and temporal variability of salinity are derived from monthly gridded maps, and the spatial patterns of the trends in the North Atlantic are compared among different products. A discussion of commonalities and differences is followed by an in-depth consideration of the Roemmich–Gilson product, which is restricted to regions well sampled by the Argo network (Roemmich and Gilson 2009).

The monthly salinity fields from the Roemmich–Gilson data produce general patterns of salinity in the North Atlantic that allow for comparison between regions and a determination of whether the different regions covary and how they differ. To shed more light on

the underlying mechanisms of these variations in salinity, the reanalysis product of evaporation minus precipitation is compared to observed trends in salinity. Furthermore, the possible relationship between salinity trends in the western subpolar gyre (SPG) and the SPG strength is investigated, as well as to what extent these might be linked to wind stress curl and climate indices such as the North Atlantic Oscillation (NAO) and the Arctic Oscillation (AO). Freshwater sources affecting salinity that were not explicitly considered in this study include those from the outflow from the Arctic Ocean, river discharge, and glacier melt from Greenland. Recent studies suggest that changes in freshwater outflow from the Arctic through the Fram and Davis Straits are not statistically significant (Haine et al. 2015).

2. Methods

This study focuses on the upper ocean of the northern North Atlantic, using monthly mean fields for the region that corresponds to the North Atlantic, including the subarctic seas and parts of the Arctic Ocean (10° – 88° N, 85° W– 35° E). Two types of products are analyzed: one subset includes purely observation-based OA products; the other selection includes reanalysis products based on an ocean model with assimilation of hydrographic data, including Argo T - S profiles. The different products have varying spatial resolutions and available periods of coverage. In all cases, the products are monthly mean fields, and the spatial resolution is at least 1° by 1° .

The obtained OA products are Roemmich–Gilson (RG) (Roemmich and Gilson 2009) from 2004 to 2015, JAMSTEC gridpoint value of the monthly objective analysis using the Argo data (MOAA GPV) (Hosoda et al. 2008) from 2001 to 2015, IPRC for 2005 to 2015, Met Office Hadley Centre HadOBS EN4 (Good et al. 2013) for 1900 to the 2015, In Situ Analysis System (ISAS-13) (Gaillard et al. 2016) from 2002 to 2012, Coriolis Ocean Dataset for Reanalysis (CORA5.0) (Gaillard et al. 2016) from 1990 to 2015, Barnes objective analysis (BOA)-Argo (Li et al. 2017) from 2004 to 2015, and Armor3D (Guinehut et al. 2012) from 1993 to 2015. The reanalysis products are the Global Ocean Reanalyses and Simulations (GLORYS2V4) from 1993 to 2015 and ECCOv4r3 (Forget et al. 2015) from 1992 to 2015. While most products provide data for all parts of the ocean, RG, JAMSTEC MOAA GPV, IPRC, and BOA-Argo are limited to regions well-sampled by the Argo network. Most OA products are updated on a regular basis to include monthly fields that follow the original release. The original release of ISAS-13 spans years 2002–2012, but there is a separate dataset that was used to extend the original ISAS-13 dataset to 2015. The selection of

TABLE 1. List of OA and reanalysis products evaluated in this study.

Name	Source	Reference	Method
Roemmich–Gilson	Scripps Institution of Oceanography (SIO) (http://sio-argo.ucsd.edu/RG_Climateology.html)	Roemmich and Gilson (2009)	OA using Argo-only data
JAMSTEC MOAA GPV	Japan Agency for Marine-Earth Science and Technology (JAMSTEC) (ftp2.jamstec.go.jp/pub/argo/MOAA_GPV)	Hosoda et al. (2008)	OA using Argo, TRITON and CTD data
IPRC	International Pacific Research Center (IPRC) (http://apdrc.soest.hawaii.edu/projects/Argo)	—	OA using Argo and altimetry data
HadOBS EN4	Met Office (http://hadobs.metoffice.com/en4)	Good et al. (2013) Gaillard et al. (2016)	OA using available hydrographic data OA using available hydrographic data
ISAS-13	Institut Français de Recherche pour l'Exploitation de la Mer (IFREMER) (http://www.ifremer.fr/lpo/content/view/full/71089)	—	—
CORA5.0	Coriolis Marine Environment Monitoring Service (CMEMS) (http://www.ifremer.fr/lpo/content/view/full/71089)	Cabanes et al. (2013)	OA using available hydrographic data
BOA-Argo	South China Sea Institute of Oceanology (SCSIO) (http://www.argo.org.cn)	Li et al. (2017) Guinehut et al. (2012)	Barnes OA using Argo only data Regression and objective analysis using Argo and satellite observations
Armor3D	CMEMS (http://marine.copernicus.eu)	von Schuckmann et al. (2016) Forget et al. (2015)	Reanalysis Reanalysis
GLORYS2V4	CMEMS (http://marine.copernicus.eu)	von Schuckmann et al. (2016)	Reanalysis
ECCOv4r3	Estimating the Circulation and Climate of the Ocean (ECCO) (http://www.ecco-group.org)	Forget et al. (2015)	Reanalysis

TABLE 2. Temporal and spatial resolutions of the different monthly gridded salinity products used in this study. Spatial resolution is based on regular latitude-longitude grids. GLORYS2V4 and ECCOv4r3 are interpolated to a regular grid. (Note: 1 dbar = 10^4 Pa.)

Name	Temporal range	Horizontal resolution	Vertical resolution; depth span	Upper levels ^a
Roemmich–Gilson	2004–15	$1^\circ \times 1^\circ$	58 levels; 0–2000 dbar	2.5, 10, 20 dbar
JAMSTEC MOAA GPV	2001–15	$1^\circ \times 1^\circ$	25 levels; 10–2000 dbar	10, 20 dbar
IPRC	2005–15	$1^\circ \times 1^\circ$	27 levels; 0–2000 m	0, 5, 10, 20 m
HadOBS EN4	1900–2015	$1^\circ \times 1^\circ$	42 levels; 0–5500 m	5, 15 m
ISAS-13	2002–15 ^b	$0.5^\circ \times 0.5^\circ$	152 levels; 0–2000 m	1, 3, 5, 10, 15, 20 m
CORA5.0	1990–2015	$0.5^\circ \times 0.5^\circ$	152 levels; 0–2000 m	1, 3, 5, 10, 15, 20 m
BOA-Argo	2004–15	$1^\circ \times 1^\circ$	58 levels; 0–2000 dbar	0, 5, 10, 20 dbar
Armor3D	1993–2015	$0.25^\circ \times 0.25^\circ$	33 levels; 0–5500 m	0, 10, 20 m
GLORYS2V4	1993–2015	$0.25^\circ \times 0.25^\circ$ (interpolated)	75 levels; 0–5500 m	0.5, 1.6, 2.7, 3.9, 5.1, 6.5, 8.1, 9.8, 11.8, 14.0, 16.5, 19.4 m
ECCOv4r3	1992–2015	$0.5^\circ \times 0.5^\circ$ (interpolated)	50 levels; 0–6000 m	5, 15 m

^a Levels included in the upper-ocean average.

^b The temporal range of the original version is 2002–12 and has been extended with near-real-time analysis to 2015.

gridded T – S products used in this study are listed in Table 1, and their main properties are listed in Table 2.

Subsurface density (at 300 dbar) at the center of the subpolar gyre was used as a proxy for the circulation strength of the subpolar gyre. The monthly T – S fields from RG were used to derive monthly fields of the potential density anomaly relative to 0 dbar (σ_0). Potential density anomaly calculations were done with the Gibbs SeaWater Oceanographic Package of TEOS-10 (McDougall and Barker 2011). The σ_0 is derived from conservative temperature and absolute salinity, which are taken from the RG temperature and salinity fields, respectively.

The subpolar gyre region was defined as the area within 50° – 65°N , 30° – 60°W where the ocean mean dynamic topography (MDT) is below -0.56 m . The MDT is the mean sea surface height between 1993 and 2012 referenced to the geoid and was obtained from the AVISO repository. The subpolar gyre region was further subdivided into a western (longitude $> 50^\circ\text{W}$), central ($50^\circ > \text{longitude} > 40^\circ\text{W}$), and eastern sector (longitude $< 40^\circ\text{W}$).

Daily gridded fields of the multaltimeter satellite sea level anomaly (SLA) product were downloaded from the Copernicus Marine and Environment Monitoring Service (CMEMS). The daily fields were selected for the relevant period (2004–15) and averaged to monthly mean fields. Atmospheric freshwater flux was derived from evaporation minus precipitation ($E - P$), which was obtained from the ERA-Interim global atmospheric reanalysis product (Dee et al. 2011) from 2004 to 2015. Furthermore, monthly fields of precipitation from the Global Precipitation Climatology Project (GPCP; Adler et al. 2003) and monthly fields of evaporation from the objectively analyzed air–sea fluxes (OAFlux) project (Yu 2007) were used to derive monthly fields of $E - P$ for 2004–15. Both satellite products and the ERA-Interim product were used. A known level of uncertainty is associated with reanalysis products,

particularly for precipitation (Chaudhuri et al. 2013); however, this was judged to have little impact on the estimated trends in $E - P$ relative to using satellite data.

Wind stress curl was derived from wind velocity fields also obtained from ERA-Interim from 2004 to 2015 rather than from a scatterometer wind stress product. ERA-Interim daily wind velocity fields were chosen because scatterometer data are unavailable after the November 2009 QuikSCAT satellite hardware failure and also because daily scatterometer fields have large spatial gaps that require optimal interpolation, which is prone to significant errors. Vector wind stress fields were calculated as $\tau = \rho_{\text{air}} C_D u^2$, where τ is either the zonal (τ_x) or the meridional (τ_y) vector wind stress field, ρ_{air} is the density of air (1.225 kg m^{-3}), C_D is the drag coefficient after Yelland and Taylor (1996), and u is either zonal or meridional vector wind velocity field. Finally, a 9-point finite difference scheme was used to calculate the curl of the wind stress from τ_x and τ_y . The wind stress curl fields from ERA-Interim were assessed using the Centre ERS d'Archivage et de Traitement (CERSAT) mean wind field (MWF) QuikSCAT product (<ftp://ftp.ifremer.fr/ifremer/cersat/products/gridded/mwf-quikscat/>), which uses the same 9-point finite difference scheme. There was a high level of agreement between wind stress curl calculated with ERA-Interim wind fields and the wind stress curl presented in CERSAT MWF QuikSCAT. Monthly time series of NAO and AO were obtained from the NOAA/ESRL Physical Sciences Division website (<https://www.esrl.noaa.gov/psd/data/climateindices/list/>).

3. Results

a. Salinity trends and variability

Data arrays of monthly salinity fields were subsetted for the 11-yr period from 2005 to 2015, and then for each

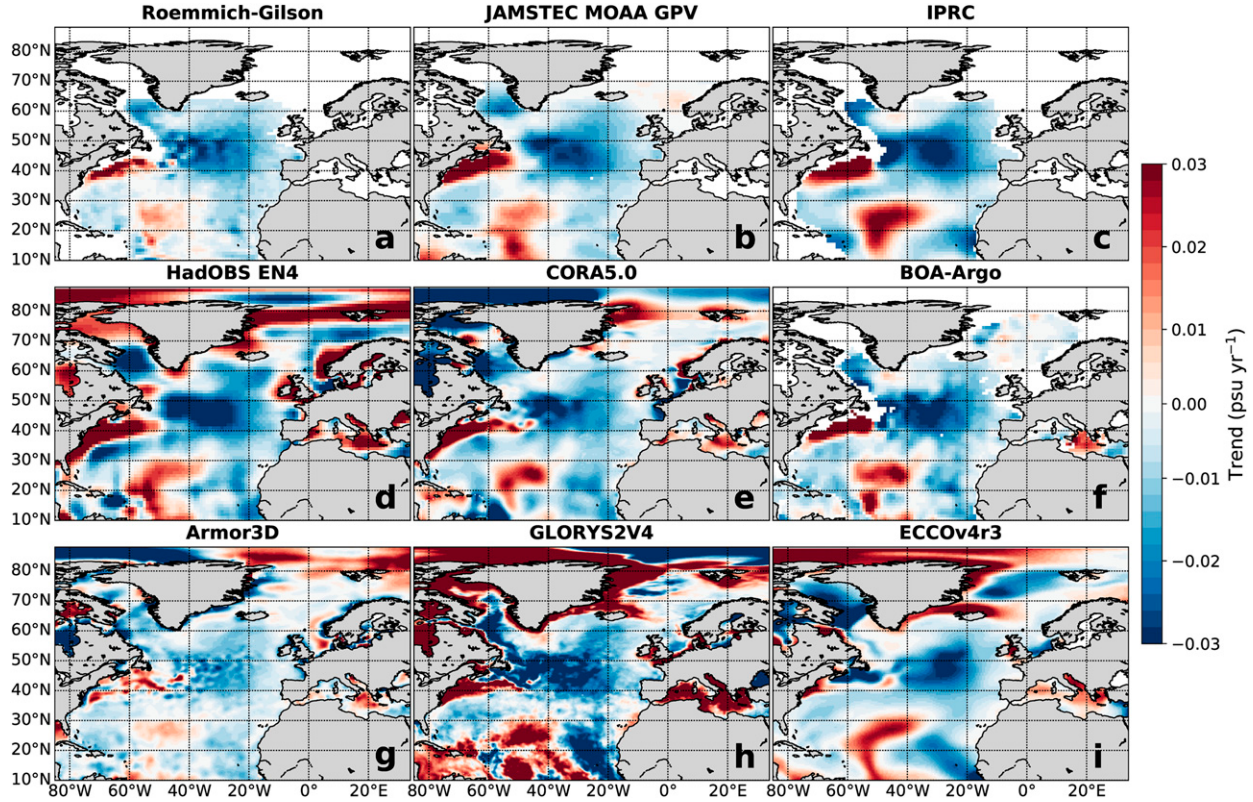


FIG. 1. Spatial distributions of linear trend in surface salinity seasonal anomaly for 2005–15 using monthly mean fields of OA and reanalysis products; OAs: (a) Roemmich and Gilson, (b) JAMSTEC MOAA GPV, (c) IPRC, (d) HadOBS EN4, (e) CORA5.0, (f) BOA-Argo, and (g) Armor3D and reanalyses: (h) GLORYS2V4 and (i) ECCOv4r3.

grid point the linear trend was calculated using a simple least squares regression fit. To minimize the influence of seasonality from the trend, the 2005–15 mean climatological seasonal cycle from each individual product was calculated and then removed from that particular product. The 2005–15 period was selected because each of the products provides sufficient coverage over this time period. This relatively short period was chosen in order to compare the monthly trend in surface salinity in all available products, and it is not expected that these trends are representative of decadal time scales. Here, surface salinity was defined as the average of the upper depth/pressure levels down to 15–20 m or dbar (Table 2). Since the multiple products have differing defined depth layers, an average of the upper 20 m or dbar allowed for a more meaningful comparison among products. There are inherent limitations to averaging salinity values over multiple depth layers, given that the uppermost layer is most strongly influenced by meltwater. However, separate analyses with only the upper layers or shallower ranges (0–10 m or dbar) did not yield any noticeable differences in the spatial trends.

The most obvious pattern represented in this data during the 2005–15 period is a decrease in surface salinity in the central North Atlantic. This decrease in salinity is present among all products (Fig. 1) and reaches from the SPG down to around 35°N. The second negative trend that occurs consistently among the products is in the Labrador Sea. A minor departure from this pattern can be observed in ECCOv4r3, which does not show a distinct negative trend in the Labrador Sea. It is not clear whether the trend in the Labrador Sea is related to the trend in the central North Atlantic.

The products also show discrepancies in their salinity trends. HadOBS EN4 and GLORYS2V4 show salinification in the Baffin Bay, where ECCOv4r3 shows freshening. CORA5.0 shows freshening in the northern Labrador Sea and no trend in Baffin Bay. Armor3D shows a similar spatial pattern to the other products, including the freshening of the Labrador Sea/Baffin Bay region, but the trend values are much smaller. Along the southern and western coast of Greenland, the trend in ECCOv4r3 and GLORYS2V4 is positive, whereas the trend in ISAS-13, and to a lesser extent in Armor3D, is negative. In the Nordic seas, most products show a

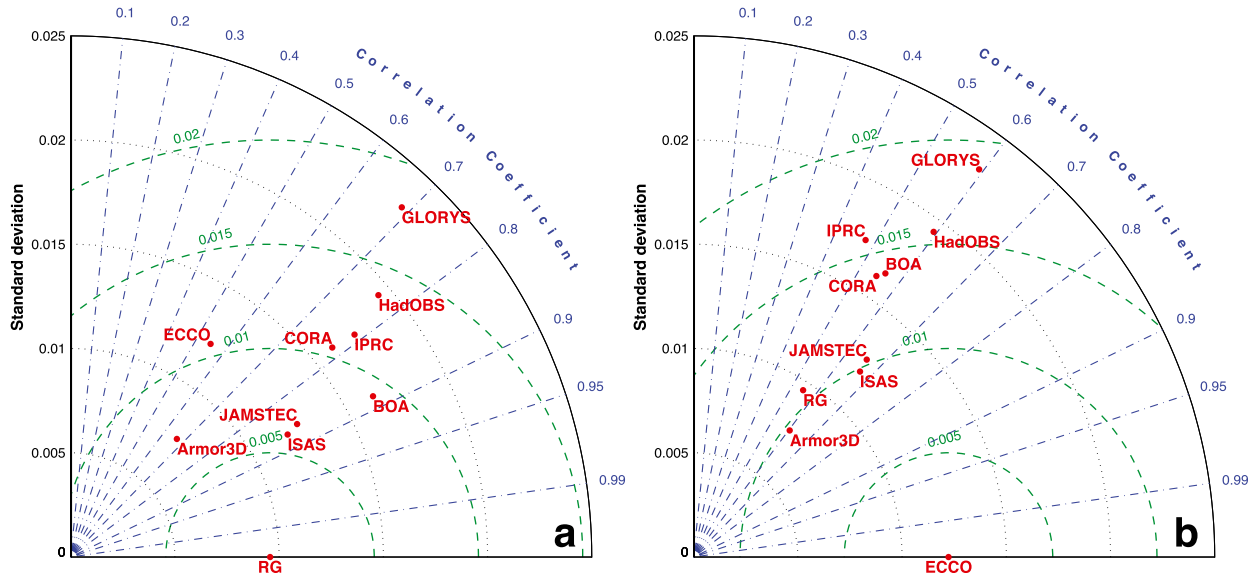


FIG. 2. Taylor diagram comparing distributions of linear trend in upper salinity anomaly (2005–15) of OA and reanalysis products. The spatial patterns are compared to the one from (a) Roemmich and Gilson and (b) ECCOv4r3.

positive salinity trend. In general, there is greater disagreement both among reanalysis products (GLORYS2V4 and ECCOv4r3) and between reanalysis and OA products than there is among OA products. A Taylor diagram of the spatial distributions in linear trends (Fig. 2a) shows all OA fields around a correlation of 0.8 to 0.9 (with similar standard deviations and RMS values), using the spatial trend from RG as a reference. The reanalysis products have lower correlations of less than 0.7 when compared to RG. Also, when comparing the spatial trends of the products against ECCOv4r3, the other reanalysis product (GLORYS2V4) shows one of the largest disagreements (with the exception of IPRC) in comparison to the OA products (Fig. 2b). Note that the Taylor diagrams have been determined only for overlapping regions across the different products.

It is important to note that large data gaps exist in some of the OA products. These mostly correspond to regions where Argo floats are largely absent or coverage is insufficient. RG and IPRC lack data in coastal regions, while RG, JAMSTEC MOAA GPV, and IPRC lack data beyond 65°–70°N. Consequently, many of the differences that are observed between the datasets are likely the result of the different interpolation methods used to estimate fields in regions with sparse data (Good et al. 2013; Gaillard et al. 2016). Nonetheless, in regions where Argo profiles are abundant, which includes most of the Labrador Sea and the central North Atlantic, the products are in good agreement. All products are defined in the tropics (south of 30°N); however, the signals are less consistent relative to the higher latitudes.

The analysis of surface salinity was also extended by examining a subset of OA products (RG, JAMSTEC MOAA GPV, HadOBS EN4, and ISAS-13) providing monthly fields from 2004 to 2015. The linear trend in surface salinity was calculated from 2004 to 2015, and, as done previously, the climatological seasonal cycle was calculated, over this longer, 12-yr period, and was removed before the trend was determined for each grid point. The general result obtained from this subset of OA products is the same; that is, the salinity has declined in large parts of the northern North Atlantic (Fig. 3). In particular, negative trends are clearly observed in the Labrador Sea and the central North Atlantic, which would therefore suggest that the signal in this region is robust. It is also apparent in each of the selected datasets that the decline in salinity is greatest in the surface waters of the western subpolar region compared to the eastern subpolar region. Farther south, the presence of a strong increase in salinity is visible off the east coast of North America in each of the datasets, which could be due to a northward shift of the western boundary current as was previously alluded to by Gawarkiewicz et al. (2012), Johnson and Lyman (2016), and Bisagni et al. (2017).

Figure 4 shows the ratio of the linear trend to its 95% confidence interval, which is based on the Student's *t* distribution. In regions where the magnitude of the ratio is larger than 1.0, the linear trend can be considered significantly different from zero. White ocean areas indicate where the linear trend cannot be considered significantly different from zero. As can be seen in Fig. 4,

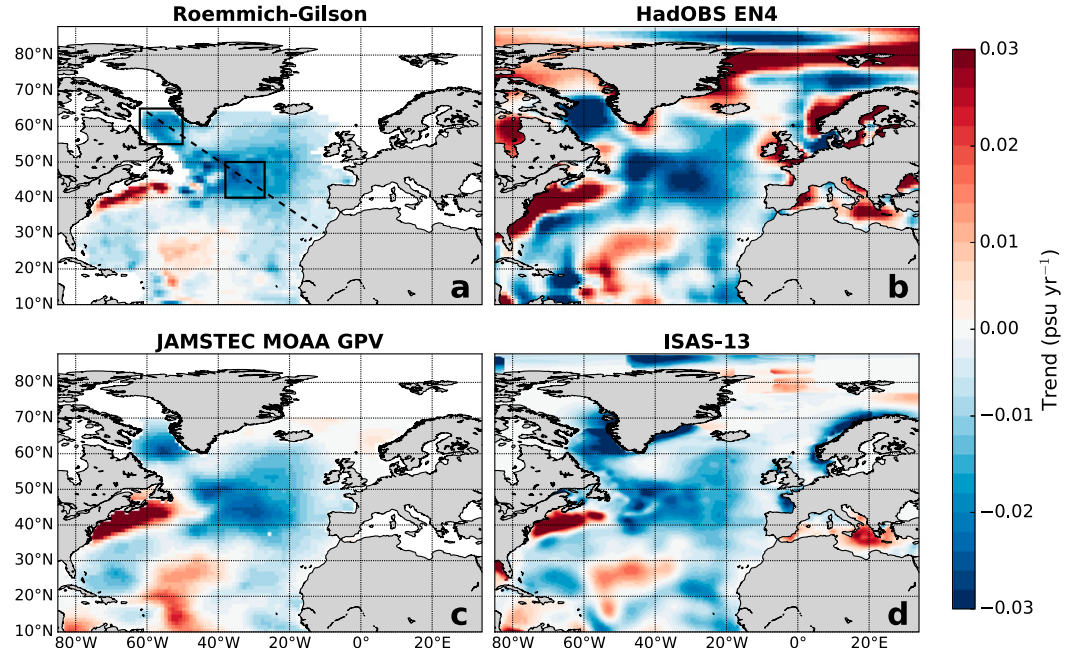


FIG. 3. Spatial distributions of linear trend in upper salinity seasonal anomaly for 2004–15 using monthly mean fields of (a) Roemmich and Gilson, (b) HadOBS EN4, (c) JAMSTEC MOAA GPV, and (d) ISAS-13. Black boxes in (a) depict the Labrador Sea (55° – 65° N, 50° – 62° W) and central North Atlantic (40° – 50° N, 27° – 38° W), from which time series of upper salinity are presented in Fig. 7. The dashed line in (a) depicts the vertical section that is presented in Fig. 8.

the linear trends in salinity are significant for most of the North Atlantic. However, the significance of the trend does not scale with the magnitude of the trend displayed in Fig. 3. Even though the trend is much weaker in the eastern half of the North Atlantic, the trend is much more significant. The difference in significance is due to the underlying pattern of interannual variability in the North Atlantic, which is much greater in the western region than in the eastern region. Thus, to better classify the overall negative trend, it is important to look at how surface salinity in the North Atlantic varies both in time (intra- and interannually) and in space.

In general, the reliability of the observed trends depends on the availability of data both in time and space. In the decade following the beginning of the Argo project (starting around 2000), the number of temperature and salinity observations per month has increased severalfold throughout much of the North Atlantic (Fig. 5). This has greatly reduced some of the temporal and spatial biases in the temperature and salinity datasets in the affected regions. A comparison of the average number of salinity profiles per 1° by 1° cell between Argo and other datasets (i.e., shipboard observations) illustrates the extent to which Argo has become a major contributor to the number of salinity observations being made in the North Atlantic and the SPG (Fig. 5d).

However, as can be seen in Fig. 5c, data coverage in the North Atlantic is still quite heterogeneous. Even with the considerable expansion of the Argo program in the last 5 years, there are still regions of the North Atlantic that remain largely undersampled.

Given the temporal and spatial distribution of available in situ observations during the last 10 years, which are mainly provided by Argo profiling floats, it seemed prudent to focus this analysis of OA products on regions where the number of in situ observations is high enough to yield accurate monthly gridded fields. For some of the OA products examined here, the lack of in situ data coverage leads to high levels of uncertainty. Furthermore, some OA methods relax to a climatology (e.g., Good et al. 2013) when there are no observations available. As a result, despite having generally similar underlying input of in situ observations, calculated trends can be very different in regions with limited data coverage (Figs. 1 and 3). To avoid such problems, further analyses of the trends and interannual variability of salinity was restricted to the RG domain (Fig. 5a), where Argo profiles are abundant and analysis errors are low. After comparing the fields of the nine available products, the RG product was chosen as the focus product since it has been generated only for regions with good data coverage. It is expected that the results of the

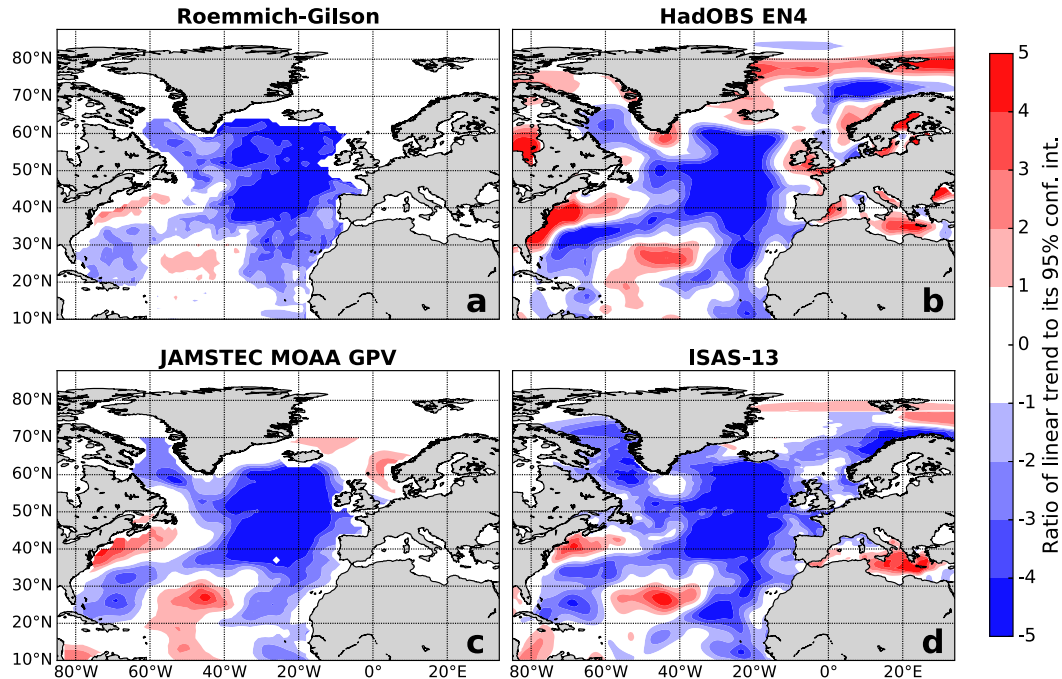


FIG. 4. Ratio of linear trend to its 95% confidence interval using monthly mean fields from 2004 to 2015 with seasonality removed as given by (a) Roemmich and Gilson, (b) HadOBS EN4, (c) JAMSTEC MOAA GPV, and (d) ISAS-13. The ratio indicates the significance of the trend, with significant trends corresponding to ratios with magnitudes larger than 1.0.

further analysis are equivalent when using other OA products within the RG domain.

As noted above, in order to classify the overall negative salinity trend, it is critical to quantify how surface

salinity in the North Atlantic varies in time and space. To this end, the monthly salinity fields of the RG product between 2004 and 2015 were used to assess spatial patterns of seasonality and interannual variability in the

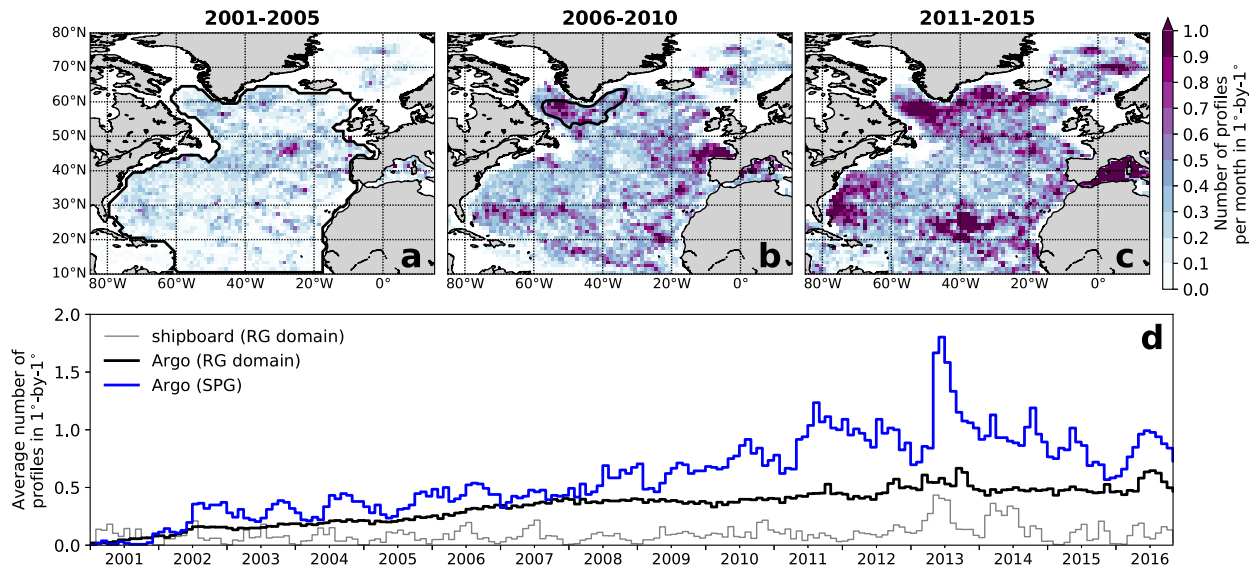


FIG. 5. The average number of Argo profiles for each month per $1^\circ \times 1^\circ$ over (a) 2001–05, (b) 2006–10, and (c) 2011–15. The monthly average of Argo and shipboard profiles per $1^\circ \times 1^\circ$ is presented in (d) for the RG domain, as outlined in (a), and the subpolar gyre region, as outlined in (b). The black outline in (a) depicts the domain where RG includes data. The black outline in (b) depicts the subpolar gyre region defined in this study based upon a threshold of MDT less than -0.56 m . The information on the number of Argo and shipboard profiles is obtained from HadOBS EN4 (<http://hadobs.metoffice.com/en4>).

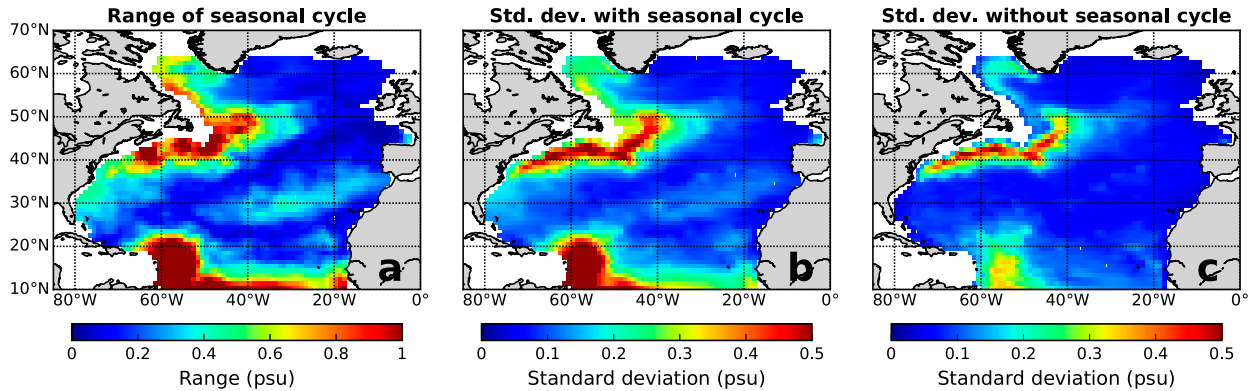


FIG. 6. Seasonality and interannual variability of salinity in the North Atlantic from 2004 to 2015 using RG monthly fields in terms of (a) the range of seasonal cycle from 0 to 1 psu and the standard deviation from 0 to 0.5 psu (b) with and (c) without the seasonal cycle.

North Atlantic. The seasonal range of salinity in the North Atlantic is high off the east coast of North America (Fig. 6a), likely corresponding to the large variability of the shelfbreak front (Linder and Gawarkiewicz 1998; Fratantoni and Pickart 2003). There is also a large seasonal cycle in the northwest Atlantic due to variability of the North Atlantic Current (NAC) (Roessler et al. 2015). On the other hand, the seasonal range is much lower in the eastern North Atlantic. Likewise, the seasonal range of salinity in the interior of the SPG is much higher in the western part compared to the eastern part. It should be noted that this difference in seasonal ranges is only applicable to the interior of the gyre, because the RG dataset does not seem to capture variability associated with the East and West Greenland Currents.

The spatial pattern of the standard deviation (Fig. 6b) is almost identical to that of the seasonal range, suggesting that the standard deviation is largely a function of seasonal range. A similar spatial pattern can be seen in the interannual variability of salinity in the North Atlantic, represented by the standard deviation of salinity with the climatological seasonal cycle removed (Fig. 6c). Interannual variability is high along the western boundary current and in the western part of the SPG, in the Labrador Sea, and relatively lower in the central to eastern North Atlantic, including the central and eastern SPG. However, there is a notable difference in the spatial pattern between the seasonal range and interannual variability. Specifically, toward the western edges of the Labrador Sea, the seasonal range of salinity is high, but the interannual variability is low. It is only farther east, into the SPG, that interannual variability is elevated. In lower latitudes the seasonal range of salinity is high throughout the tropics, whereas interannual variability is much higher in the western tropics.

Salinity in the Labrador Sea has a distinct seasonal cycle reflecting the formation and melting of sea ice in

winter and summer months, respectively (Lazier 1980; Straneo 2006). During the summers of 2008 and 2012, excursions from this seasonality were particularly strong (Figs. 7a,c). However, in the central North Atlantic, the large negative anomalies that we see in the Labrador Sea in 2008 and 2012 are absent (Figs. 7b,d). In addition, while a seasonal cycle of surface salinity can be observed in the central North Atlantic, the amplitude of that cycle is considerably reduced, as compared to the Labrador Sea, though the magnitude of the underlying negative trend for salinity with seasonality removed is nearly the same in both regions (-0.017 ± 0.005 and $-0.020 \pm 0.003 \text{ psu yr}^{-1}$ for Labrador Sea and central North Atlantic, respectively).

Another distinct difference between regional salinity trends is that the negative trend is also observable at much deeper depths in the east compared to the west. A vertical section of the linear trend (Fig. 8) from the northwest corner of the Labrador Sea ($64^\circ\text{N}, 60^\circ\text{W}$) down to the coast of northwestern Africa ($30^\circ\text{N}, 10^\circ\text{W}$) shows that the decrease in salinity is only concentrated in the upper 100 dbar in the Labrador Sea ($50^\circ\text{--}60^\circ\text{W}$), while the negative trend can be observed to deeper than 500 dbar farther east in the central part of the North Atlantic ($25^\circ\text{--}45^\circ\text{W}$). The pressure-longitude section (Fig. 8), as well as the latitude-longitude maps (Fig. 3a), of the RG-derived salinity trend reveals a clear discontinuity between the two regions of predominant negative trends. This discontinuity lies across the NAC, suggesting that the trends in the two regions are driven by independent forces.

When the linear trend in the North Atlantic is broken down into two different time periods (2004–10 and 2010–15; Fig. 9), further differences emerge with respect to the trends that are observed in the central and eastern North Atlantic compared to the SPG and Labrador Sea. In 2004–10, there is a clear negative trend in the SPG,

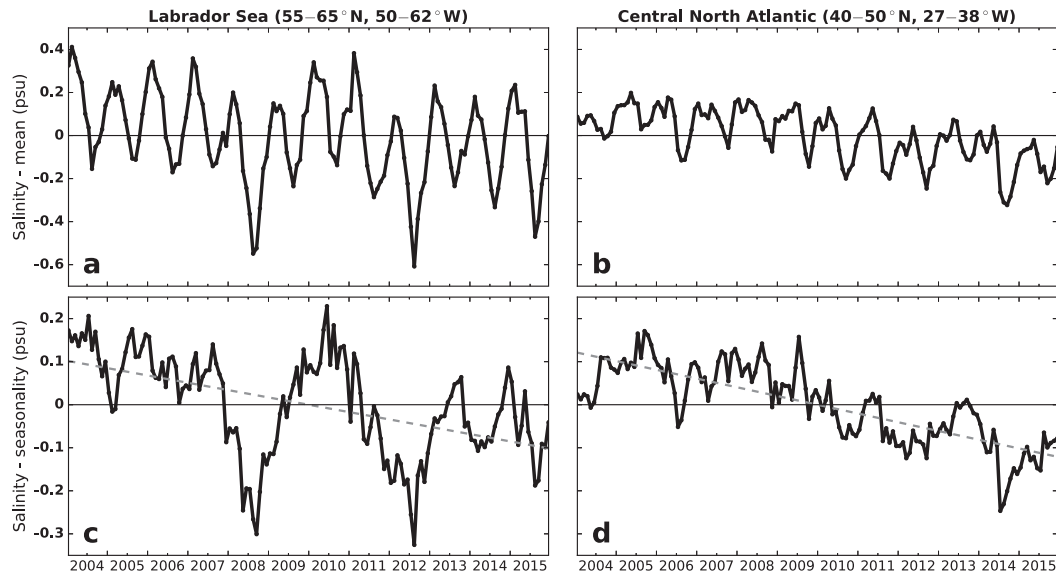


FIG. 7. Time series of mean salinity in the upper 20 m averaged over (a),(c) the Labrador Sea and (b),(d) central North Atlantic using RG monthly fields. The two regions are outlined in Fig. 3a. Time series are presented both (a), (b) with and (c),(d) without seasonal cycle. A linear regression (gray dashed lines) yields a slope of $-0.017 \pm 0.005 \text{ psu yr}^{-1}$ for (c) the Labrador Sea and $-0.020 \pm 0.003 \text{ psu yr}^{-1}$ for (d) the central North Atlantic.

especially in the western part and in the Labrador Sea. Salinity trends in the eastern North Atlantic are relatively weak or nonexistent from 2004 to 2010, whereas in 2010–15, the trend is negative in much of the eastern North Atlantic. In 2010–15, the negative trends are considerably more pronounced both in the Labrador Sea and the eastern North Atlantic and positive in the western boundary current and central SPG. Figures 9c,d also reveal that in 2004–10, the negative salinity trend in the western North Atlantic occurs in only the upper 100–200 dbar. In contrast, in 2010–15, a negative trend is observed from the surface down to around 1800 dbar throughout most of the northwest Atlantic, including the

Labrador Sea. The reversal of the salinity trend in the deeper (200–1800 dbar) Labrador Sea, which is positive in 2004–10 and negative in 2010–15, is likely the result of increasing deep convection in the Labrador Sea (Yashayaev and Loder 2017) bringing fresher surface water deeper into the Labrador Sea. The negative trends evident during 2010–15 in the deeper layers (down to 1000 dbar) of the central North Atlantic are likely due to reduced salt transport from the NAC as a result of a weakening Atlantic meridional overturning circulation (AMOC) (Robson et al. 2016). In contrast, the negative trends evident in the Labrador Sea that are of the same magnitude as in the central North Atlantic are restricted

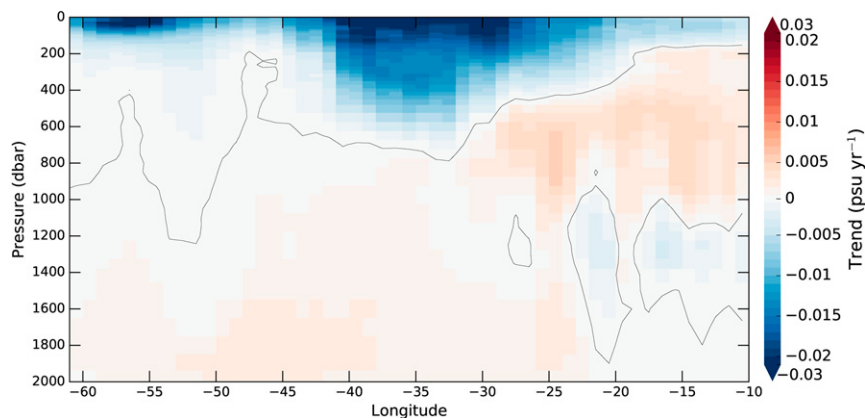


FIG. 8. Linear trend of salinity evaluated from the RG OA product for a vertical section across the North Atlantic, from 64°N, 60°W to 30°N, 10°W as shown in Fig. 3a.

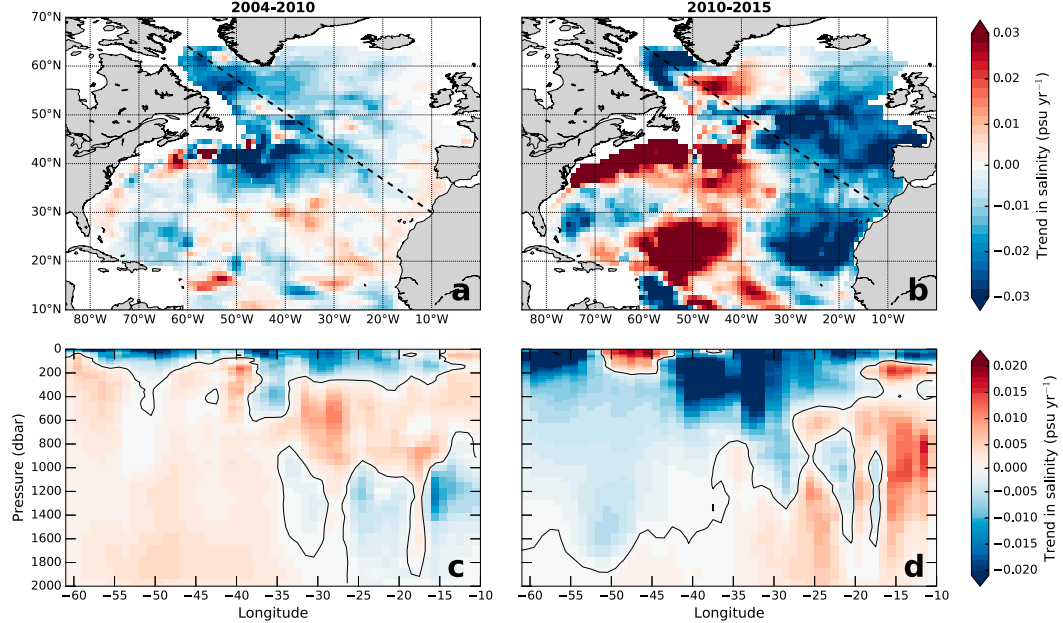


FIG. 9. Spatial pattern of linear trends in salinity in the North Atlantic for the time periods (a), (c) 2004–10 and (b), (d) 2010–15 derived from the RG dataset. The spatial distribution of the salinity trends in the upper 20 m for (a) 2004–10 and (b) 2010–15. Dashed lines indicate the location of the vertical section shown in (c) and (d). The linear trend in salinity of a vertical section across the North Atlantic (from 64°N, 60°W to 30°N, 10°W) for (c) 2004–10 and (d) 2010–15.

to the upper 200 dbar, with negative trends of much smaller magnitude observed deeper in the Labrador Sea.

A distinction between east and west is also observable in the subpolar North Atlantic. Within the SPG, the trends and interannual variability of salinity vary substantially between the western section and the central and eastern sections (Fig. 10). Interannual variability in the central and eastern SPG is much lower compared to the western part, which is part of the Labrador Sea. In

addition, the central and eastern SPG regions do not show the large negative excursions in 2008 and 2012 that are observed in the western SPG. Similarly, a negative salinity anomaly in 2015, in which the summer months were anomalously fresh, was observed only in the western SPG. A small negative anomaly in 2010 is detectable in both the central and eastern SPG, which is not apparent in the western SPG. The long-term spatial trend in the SPG (Fig. 10a) suggests that the freshening

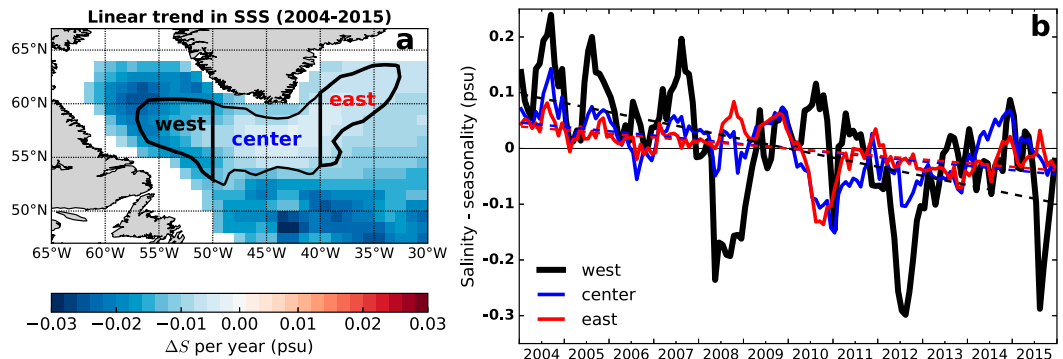


FIG. 10. Linear trend and interannual variability of salinity in the SPG. (a) Linear trend in upper salinity from 2004 to 2015 as given by monthly anomaly fields derived from the RG dataset. (b) Time series of upper salinity with the seasonal cycle removed. Salinity is spatially averaged over three different parts of the SPG, defined as west (black), center (blue), and east (red). Linear regression lines are shown as dashed lines for each region (west: -0.016 ± 0.004 psu yr^{-1} ; center: -0.008 ± 0.002 psu yr^{-1} ; and east: -0.007 ± 0.002 psu yr^{-1}).

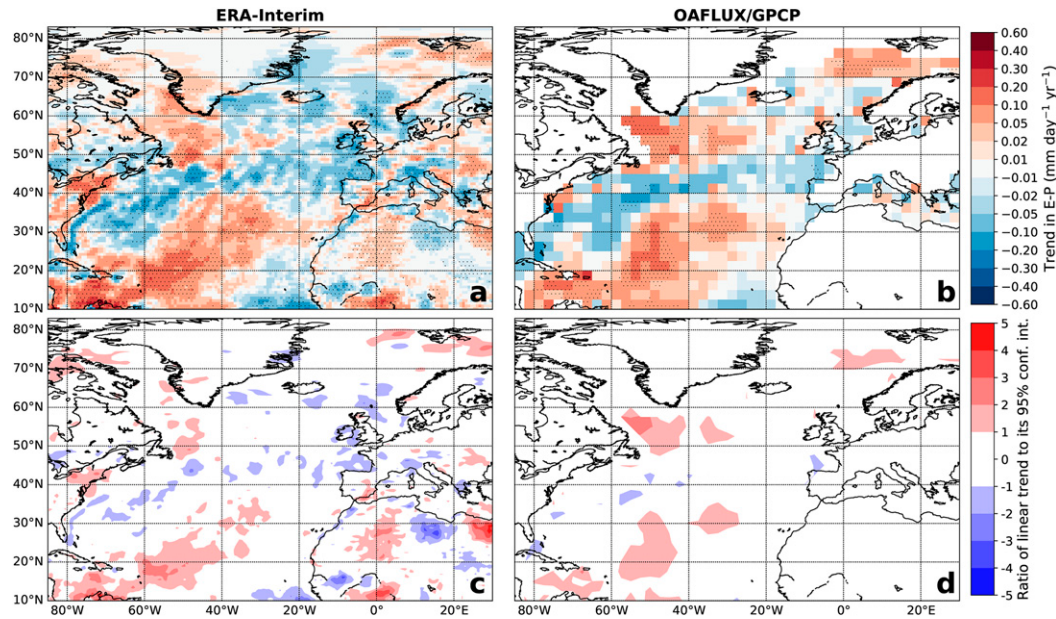


FIG. 11. Spatial distribution of linear trend in $E - P$ from 2004 to 2015 derived from (a) ERA-Interim and (b) OAFlux/GPCP evaporation and precipitation data. The mean seasonal cycle was removed before the trend was calculated. (c),(d) Ratio of linear trend to its 95% confidence interval using monthly mean fields of $E - P$ from 2004 to 2015 with seasonality removed as given by ERA-Interim and OAFlux/GPCP, respectively. The stippling in (a) and (b) indicates regions where the magnitude of the ratio of the linear trend to its 95% confidence interval is larger than 1.0.

signal in the western SPG is stronger. Based on the slopes of the linear fits of the spatially averaged time series (Fig. 10b) the linear trend in the western part ($-0.016 \pm 0.004 \text{ psu yr}^{-1}$) is twice that of the central and eastern parts of the SPG (-0.008 ± 0.002 and $-0.007 \pm 0.002 \text{ psu yr}^{-1}$ for the central and east, respectively).

b. Mechanisms

One of the main factors affecting the spatial pattern of surface salinity in the ocean is the difference between evaporation and precipitation. In the subpolar region, precipitation exceeds evaporation over time so that long-term mean $E - P$ is negative; this process is balanced by the net advection of salt from lower latitudes. The $E - P$, however, could be affected by an acceleration of the global hydrological cycle (Durack et al. 2012), which would cause greater precipitation relative to evaporation in the subpolar North Atlantic. On the other hand, an acceleration of the hydrological cycle would also lead to higher salinities in the subtropics and consequently to increased net salt transport to the subpolar regions. On the basis of an examination of this trend in the reanalysis and satellite derived $E - P$ from 2004 to 2015 (Fig. 11), it does not appear that there is an increasing imbalance between precipitation and evaporation in the western SPG and Labrador Sea. In fact, the

trend in $E - P$ is slightly positive, suggesting that changes in $E - P$ are not a factor in explaining the negative trend in salinity in the northwest Atlantic. An increased air-sea freshwater flux and possible freshening of the sea surface are only observed in the ERA-Interim $E - P$ in the eastern SPG, where trends in salinity are not negative or are much smaller compared to the northwest Atlantic.

Ocean advection is a major factor in the relationship between air-sea freshwater flux and sea surface salinity (Yu 2011). Given the cyclonic circulation of the SPG, it cannot be ruled out that freshwater signals that developed in the eastern SPG are subsequently advected westward. In the present study, this possibility was investigated by comparing potential density σ_0 at 300 dbar $\sigma_0(300)$ within the center of the SPG with the salinity anomaly in the western sector of the SPG. The $\sigma_0(300)$ serves as a proxy for the baroclinic strength of the SPG, following the thermal wind relationship between the geostrophic velocity shear and the horizontal density gradient. Since the circulation in the SPG is cyclonic, a spinup of the gyre will cause isopycnals to dome higher in the center of the gyre. Consequently, we hypothesize larger values of $\sigma_0(300)$ are associated with stronger cyclonic circulation and would incorporate more freshwater and sea ice from the East Greenland Current.

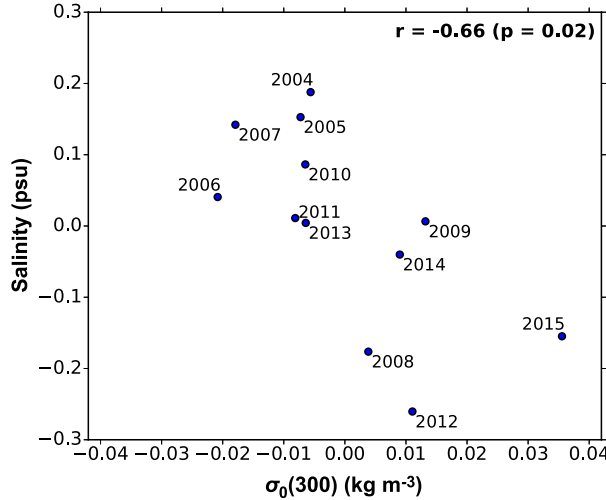


FIG. 12. Scatterplot of salinity in the western SPG against $\sigma_0(300)$ for the central SPG using the seasonal anomaly for both salinity and $\sigma_0(300)$. The spatial average of $\sigma_0(300)$ corresponds to the central gyre defined between 40° and 50°W and between 55° and 60°N where the mean $\sigma_0(300)$ is larger than 27.71 kg m^{-3} . For each year, salinity and $\sigma_0(300)$ are averaged for the months of June–October. The Pearson correlation of the June–October averages is -0.66 with a p value of 0.02 .

A negative relationship between $\sigma_0(300)$ and the western SPG salinity anomaly can be observed from June to October (Fig. 12). This demonstrates that freshening in the gyre is indeed correlated with increasing gyre strength between 2004 and 2015. It is only from June to October, when one can expect glacial and sea ice melt to occur, that salinity in the western SPG and $\sigma_0(300)$ in the central gyre show an overall negative

correlation ($r = -0.61; p = 0.036$). No such correlation is observed during the other (e.g., winter) months of the year. Also, three (2008, 2012, and 2015) of the years with the strongest circulation (2008, 2009, 2012, 2014, and 2015) are associated with negative salinity anomalies in the western SPG. Conversely, between 2004 and 2015, none of the years with a reduction in gyre strength are associated with the presence of negative salinity anomalies in the western SPG.

Besides the negative relationship with western SPG salinity anomalies during the summer months, $\sigma_0(300)$ reveals seasonal and interannual variability in SPG strength. The monthly time series of $\sigma_0(300)$ and isopycnal depth suggest that the strength of the circulation has been increasing over the last two to three years (Fig. 13). Together, the co-occurrence of gyre strengthening and negative salinity anomalies during the meltwater season suggests that gyre circulation might affect salinity by contributing to the transport of meltwater and sea ice to the western SPG and Labrador Sea. However, this only quantifies the strength of the baroclinic circulation and does not account for barotropic variability. To examine the barotropic variation in SPG circulation, a monthly time series of SLA was examined together with seasonal anomalies of $\sigma_0(300)$ and isopycnal depth (Fig. 13). Here we use values averaged over the central SPG. However, the choice of the central patch versus the entire SPG region does not have a substantial effect on the estimated values of $\sigma_0(300)$, isopycnal depth, absolute dynamic topography (ADT), or SLA.

The isopycnal depth and to a lesser degree the SLA within the SPG are anticorrelated with $\sigma_0(300)$ of the

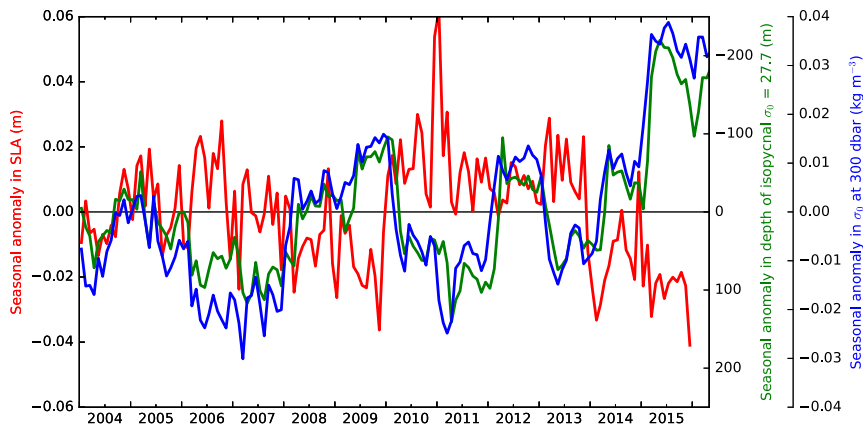


FIG. 13. Monthly time series of seasonal anomalies of $\sigma_0(300)$, isopycnal depth for $\sigma_0 = 27.7 \text{ kg m}^{-3}$, and SLA. The $\sigma_0(300)$ (blue) is averaged over the central SPG, the area of the central gyre (55° – 60°N , 40° – 50°W) where the mean $\sigma_0(300)$ is larger than 27.71 kg m^{-3} . Isopycnal depth (green) and SLA (red) are averaged over the whole subpolar gyre (i.e., where MDT $< -0.5 \text{ m}$). Isopycnal depth scale is inverted; negative anomalies represent a decline in depth and thus an uplift of the isopycnals, and positive anomalies represent an increase in depth.

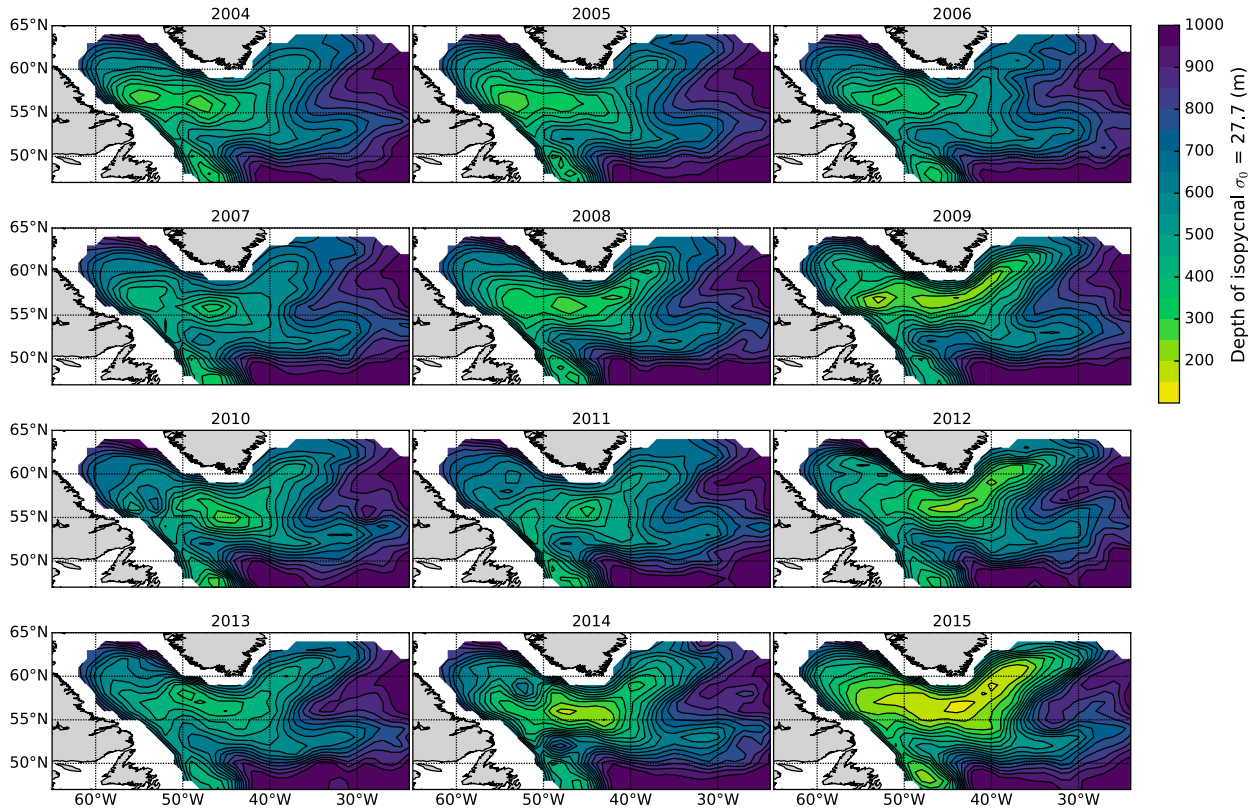


FIG. 14. Isopycnal depth for $\sigma_0 = 27.7 \text{ kg m}^{-3}$ over the SPG region. Each panel shows the spatial distributions of the mean June–October isopycnal depth for each year from 2004 to 2015. The σ_0 was derived from Roemmich–Gilson T–S fields and used to transform the dataset from pressure to isopycnal coordinates. Isopycnal $\sigma_0 = 27.7 \text{ kg m}^{-3}$ was chosen since this isopycnal is situated around 300 dbar and never outcrops between June and October during the period of 2004–15.

central gyre (Fig. 13). There is a strong anticorrelation between $\sigma_0(300)$ and isopycnal depth ($r = -0.92$) and a weak anticorrelation between $\sigma_0(300)$ and SLA ($r = -0.50$). The sea level is depressed when the gyre is spinning faster, which is associated with a larger $\sigma_0(300)$ and shallower isopycnal. Figures 14 and 15 show the June–October spatial distributions from 2004 to 2015 of the isopycnal depth for $\sigma_0 = 27.7 \text{ kg m}^{-3}$ and the ADT, respectively. The evolution of the spatial pattern clearly indicates an eastward expansion of the SPG, driven primarily by pycnocline changes (Fig. 14) rather than changes in sea level (Fig. 15).

The $\sigma_0(300)$ quantifies the strength of the baroclinic circulation, but arguably the barotropic mode also plays an important role in the SPG transport (Häkkinen and Rhines 2004; Daniault et al. 2011; Sarafanov et al. 2012). Figure 13 suggests that the barotropic and baroclinic signatures are related in that the SLA varies in the same manner as isopycnal depth at $\sigma_0 = 27.7 \text{ kg m}^{-3}$ and $\sigma_0(300)$. Further, the spatial patterns of the linear trends in isopycnal depth (at $\sigma_0 = 27.7 \text{ kg m}^{-3}$) and ADT in the SPG (Fig. 16) show that the changes in the baroclinic

mode and the barotropic mode are very similar. A scatterplot of annual means of $\sigma_0(300)$ and SLA over the central SPG demonstrates that the baroclinic and barotropic fluctuations are correlated (Fig. 17). This suggests that the western salinity anomalies are due to circulation fluctuations in both the baroclinic and barotropic flows. The sense of the $\sigma_0(300)$ and ADT relationship (anti-correlated) is to focus the circulation changes in the upper ocean, with reduced changes in the deep ocean. However, comparing Figs. 14 and 15 reveals that the barotropic variations might not play a significant role in the modulation of freshwater flux in the western SPG and Labrador Sea, because the biggest signal appears in the isopycnal depth (Fig. 14), not ADT (Fig. 15). While the barotropic mode may be dominant in the mean gyre circulation, these results indicate that year-to-year fluctuations occur in the baroclinic mode and may therefore be more relevant to the western salinity anomalies.

It has been established that one key factor controlling the variability of the SPG circulation is the variability of the overlying winds (e.g., Spall and Pickart 2003). Figure 18a shows the spatial distribution of the 2004–15

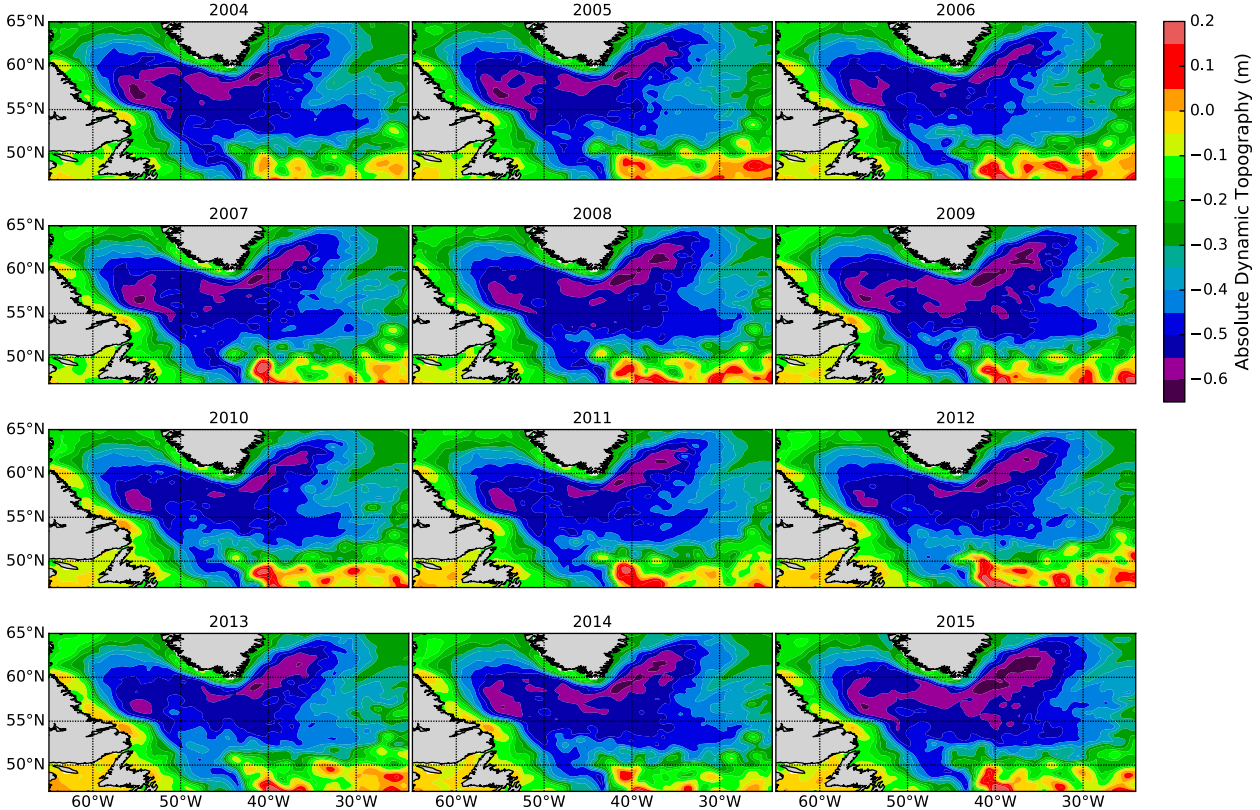


FIG. 15. ADT over the SPG region. Each panel shows the spatial distribution of the mean June–October ADT for each year from 2004 to 2015. ADT is calculated from SLA by adding the mean 1993–2012 MDT.

mean $\sigma_0(300)$, which shows elevated values in the central part of the gyre. The spatial mean of $\sigma_0(300)$ is computed over the area where the mean $\sigma_0(300)$ is larger than 27.71 kg m^{-3} , and its monthly time series is compared to variations in wind stress curl. In the present study, the wind stress curl is derived from 10-m zonal (u) and meridional (v) wind components of ERA-Interim from 2004 to 2015. The 2004–15 mean pattern of wind stress curl is generally positive in the SPG and greater in the east compared to the west (Fig. 18b). In fact, one of the highest values of wind stress curl, particularly in winter, is southeast of Greenland, associated with the Greenland tip jet (Doyle and Shapiro 1999).

A region between southeast Greenland and Iceland (57° – 68°N , 25° – 43°W), where the 2004–15 mean wind stress curl is positive, was selected to derive a monthly time series of wind stress curl. The cross correlation between anomaly of the wind stress and $\sigma_0(300)$ shows that the circulation of the SPG is correlated with positive wind stress curl in the eastern SPG (Fig. 18c). However, in this relationship, gyre strengthening is delayed by a time lag of 6–12 months (Figs. 18c,d), which is consistent with the dynamical adjustment of the SPG to variations in wind stress curl (Spall and Pickart 2003). As Fig. 18c

shows, the greatest correlation between $\sigma_0(300)$ and wind stress curl occurs when $\sigma_0(300)$ is shifted back by 12 months. The cross correlation at a lag of 1 year is 0.06, which corresponds to a Pearson correlation of 0.45 with a p value well below 0.05 (3.6×10^{-8}). Using a 5-month running mean of the wind stress curl results in a Pearson correlation of 0.74 (Fig. 18d). Consistent with the findings of Spall and Pickart (2003), we also see significant correlation between winter wind stress curl (average of January–March) and the following summer to fall $\sigma_0(300)$ (average of June–October), resulting in a correlations coefficient of $r = 0.72$ ($p = 0.008$). The strengthening of the SPG in recent years might be due to an extended period of consistent positive curl in the eastern SPG. However, the monthly averages of $\sigma_0(300)$ rise substantially during the final year, which is not mirrored by the wind stress curl in the year before. This suggests that possibly another mechanism is at play that causes the gyre to spin up more than can be explained by the wind stress curl. Interestingly, the wind stress curl in the eastern SPG covaries with the NAO and the AO index (Fig. 19), which are often considered as key variables that describe the atmospheric forcing in the North Atlantic and Arctic Ocean (Hurrell and Deser

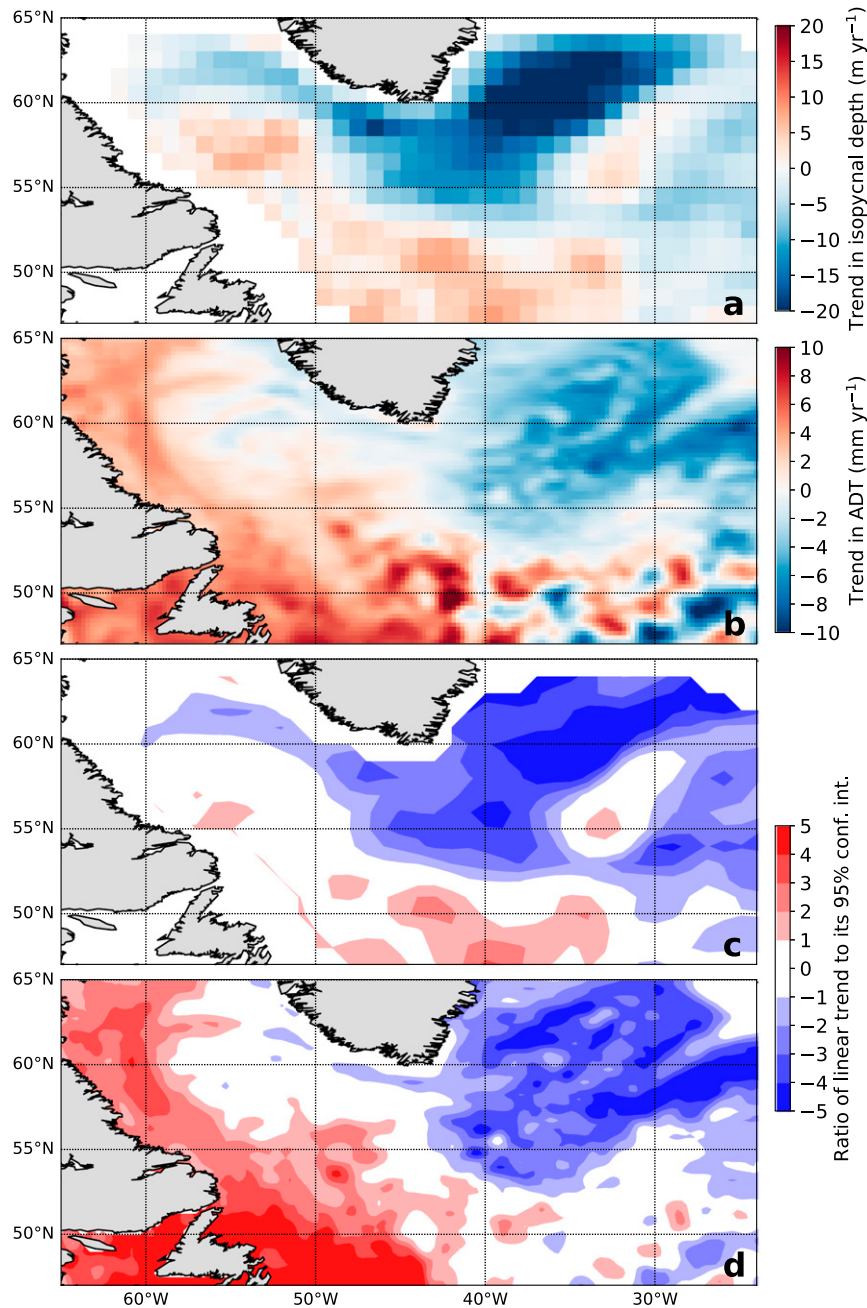


FIG. 16. Spatial distribution of linear trend in the (a) isopycnal depth (for $\sigma_0 = 27.7 \text{ kg m}^{-3}$) from 2004 to 2015 from Roemmich–Gilson T–S fields and (b) AVISO ADT from 2004 to 2015. The mean seasonal cycle was removed before the trend was calculated. Ratio of linear trend to its 95% confidence interval using monthly mean fields of (c) isopycnal depth and (d) ADT from 2004 to 2015 with seasonality removed.

2009; Houssais et al. 2007). Indeed, previous studies have long shown that most of the variability of North Atlantic circulation is related to the NAO and that the oceanic response to changes in the NAO happens at multiple time scales (Eden and Willebrand 2001; Eden and Jung 2001).

4. Discussion

Analysis of salinity products reveals large-scale negative trends in surface salinity in the North Atlantic, particularly in the central North Atlantic, the Labrador Sea, and the western subpolar region. These trends were

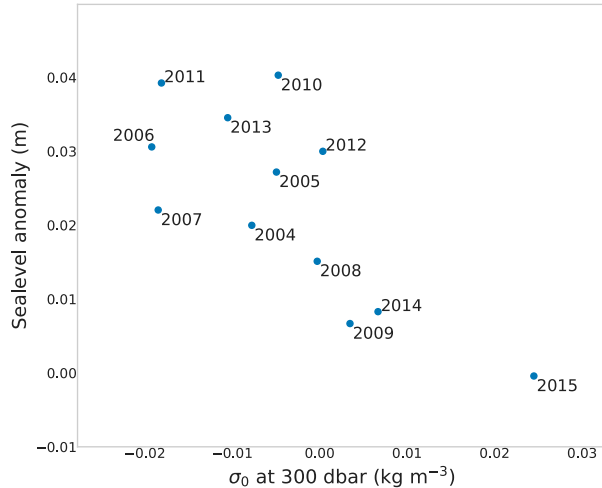


FIG. 17. Scatterplot of SLA against $\sigma_0(300)$ for the central SPG using annual means for both SLA and $\sigma_0(300)$. The spatial averages correspond to the central gyre defined between $40^{\circ}\text{--}50^{\circ}\text{W}$ and $55^{\circ}\text{--}60^{\circ}\text{N}$ where the mean $\sigma_0(300)$ is larger than 27.71 kg m^{-3} . The Pearson correlation of the annual means is -0.75 with a p value of 0.005.

universally observed across all data products over the period from 2004 to 2015. Given the 11–12-yr time scales used in this study, it is difficult to distinguish low-frequency natural variations from long-term trends due to anomalous forcing. However, existing salinity products that provide a record of 20 years or longer contain only sparse data prior to 2004 because of the limited deployment of Argo floats, leading to large uncertainties in the datasets prior to 2004. Thus, a trade-off exists between the length of the time series employed for analysis and the availability of sufficient data across that time period. Despite the trade-off, a time scale of 12 yr is not unprecedented when sampling limitations restrict a longer study, and regardless of whether the distinct freshening trends are caused by natural variation or anomalous forcing, it is important to understand the mechanisms driving these trends even over shorter time periods.

There are multiple possible mechanisms that might be contributing to the observed salinity trends. These can be categorized as either a change in freshwater sources or changes in the transport of freshwater. The terms representing freshwater sources include air-sea freshwater flux, runoff, and sea ice formation and melt. Mechanisms involved in transport include salt advection from Ekman transport, geostrophic flow, vertical entrainment, and horizontal diffusion.

The variation of mean salinity in the upper 20 m can be expressed as a mixed layer salinity budget, which is used in a range of studies (e.g., Ren et al. 2011; Schlundt et al. 2014), and may be written as

$$h \frac{\partial S}{\partial t} = -h(\mathbf{u}_e \cdot \nabla S + \mathbf{u}_g \cdot \nabla S + \kappa \nabla^2 S) - w_e \Delta S + (E - P - R + I)S, \quad (1)$$

where h is the mixed layer depth, S is the mean salinity in the mixed layer, \mathbf{u}_e is the Ekman velocity, \mathbf{u}_g is the geostrophic velocity, κ is the horizontal eddy diffusivity, w_e is the entrainment velocity, ΔS is the difference between the mean salinity of the mixed layer and the salinity just below the mixed layer, and E , P , and R are evaporation, precipitation, and runoff, respectively. The term I is the sea ice contribution, where I is positive for brine rejection during freezing and I is negative for freshening during melting. In Eq. (1), the variation in mixed layer salinity is described by the balance between salt advection from Ekman transport $\mathbf{u}_e \cdot \nabla S$, geostrophic flow $\mathbf{u}_g \cdot \nabla S$, vertical entrainment $w_e \Delta S$, horizontal diffusion $\kappa \nabla^2 S$, air-sea freshwater flux $E - P$, runoff R , and sea ice formation and melt I .

In terms of freshwater sources, there is potentially an increased runoff R in connection with an acceleration of the hydrological cycle. Furthermore, both transport of Greenland meltwater and Arctic freshwater and sea ice are potentially important terms in the salt budget of the Labrador Sea and western SPG. However, it is worth noting that freshwater fluxes through the Davis Strait and Fram Strait have not shown an obvious increase during the period of the study (Haine et al. 2015). Therefore, changes in the Arctic freshwater outflow might not be a significant factor in explaining the observed short-term salinity trends in the region and will likely only be detectable on decadal time scales with continued melting of the Arctic sea ice. Instead, it appears that the offshore transport of Greenland meltwater could be potentially impacting the salinity in the Labrador Sea (Böning et al. 2016; Luo et al. 2016; Yang et al. 2016). For example, in 2012, which was a record melting year for Greenland (Nghiem et al. 2012; Hanna et al. 2014), there was a large negative salinity excursion in the Labrador Sea (Fig. 7). In August 2012, the mean salinity of the upper 20 m was 0.34 psu below the 2004–15 climatological mean of August. The drop in salinity corresponds to a freshwater input of 11 km^3 in the upper 20 m between March and August 2012.

What caused the salinity anomalies that occurred in 2008, 2012, and 2015 in the western SPG remains an open question. Interannual variation in the offshore transport of meltwater from the coast of southwest Greenland could affect freshwater input into the Labrador Sea (Luo et al. 2016). In 2008, upwelling favorable winds led to an increased transport of meltwater from Greenland, despite the relatively low amount of runoff that year. This is consistent with observations of a

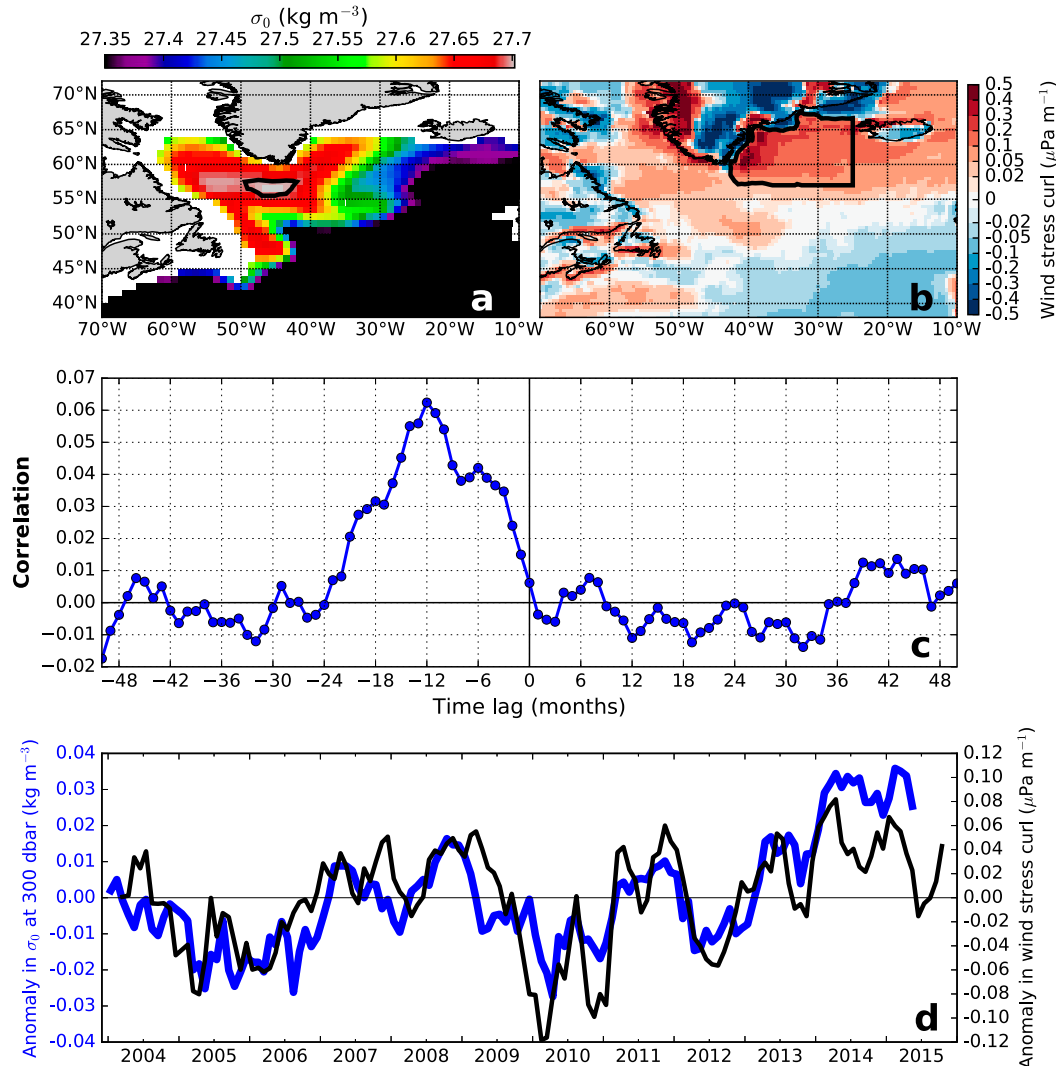


FIG. 18. (a) Spatial distribution of the 2004–15 mean $\sigma_0(300)$. The area of the central gyre where mean $\sigma_0(300)$ is larger than 27.71 kg m^{-3} is outlined in black. (b) Spatial distribution of the 2004–15 mean wind stress curl. (c) Cross correlation between wind stress curl averaged over the eastern subpolar gyre, as outlined in (b), and $\sigma_0(300)$ averaged over the central gyre, as outlined in (a). The maximum cross correlation of 0.06, occurring at time lag of -12 months, corresponds to a Pearson correlation of 0.45 ($p = 3.6 \times 10^{-8}$). (d) Time series of the 5-month running mean of wind stress curl (black) and $\sigma_0(300)$ (blue) with the time series of $\sigma_0(300)$ shifted backward by 12 months.

salinity anomaly in the Labrador Sea in the summer of 2008. In 2012, meltwater runoff was high, but offshore transport in the same year was low. Luo et al. (2016) attribute the lack of offshore transport to the presence of downwelling-favorable winds during the melting season. It is not clear whether the negative salinity anomaly that is observed in 2012 is a result of Greenland melting or other processes. Furthermore, the salinity anomalies that were observed in the Labrador Sea in 2008 and 2012 were larger over the Labrador Slope than they were on the Greenland side of the basin (Yashayaev et al. 2015). Similar freshwater events were observed in 2008 and

2013 in the Nordic seas and Barents Sea, leading Yashayaev et al. (2015) to speculate that they might have been advected into the region after the major Arctic meltwater events that had been observed the years before.

Recent studies have found a relationship between the decadal variability of the AMOC and the deep convection in the Labrador Sea (Haine 2016; Jackson et al. 2016; Robson et al. 2016), such that one can expect fresher and colder water masses in the Labrador Sea in response to the recent weakening of AMOC. In terms of ocean transport, Robson et al. (2016) argues that the freshening (and cooling) that is observed in the central

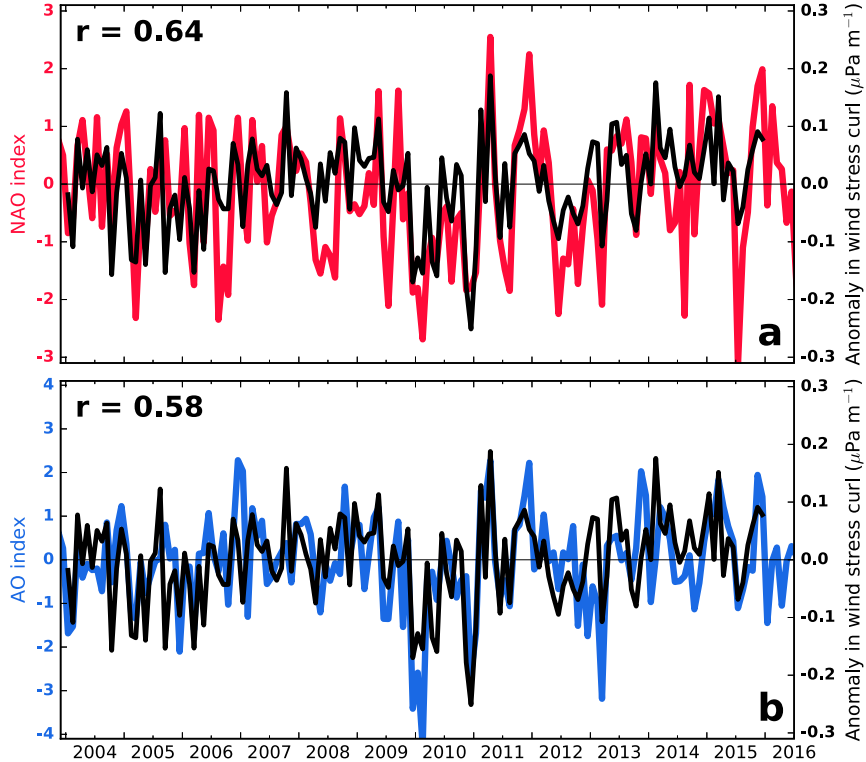


FIG. 19. Time series of anomaly in wind stress curl (black) averaged over the eastern subpolar gyre (as outlined in Fig. 18b) plotted with time series of (a) NAO (red) and (b) AO climate index (blue).

North Atlantic is consistent with a reduction in ocean circulation decreasing the northward transport of salt (and heat). Thus, recent trends in the AMOC could explain the negative salinity trends. However, this is not obvious in the western SPG where, besides a negative trend, negative excursions in salinity do not correspond to variability in the AMOC.

One indication that the negative trend in surface salinity in the Labrador Sea might not be directly linked to a weakening of the AMOC is that salinity anomalies observed in the central Atlantic and the Labrador Sea do not appear in the expected sequence, based on the general circulation of the subpolar North Atlantic. Specifically, if the AMOC is the dominant driver of the salinity decline, then such a decline would be expected first in the central North Atlantic, followed by a decline in the Labrador Sea, as the lower salinity waters from the NAC are transported to the Labrador Sea via the Irminger Current. However, in Fig. 9, one can see that the decline in salinity appears first in the Labrador Sea and is observed only later in the central North Atlantic. If the negative trend in the Labrador Sea were solely due to the advection of anomalous low salinity water (due to a weakened AMOC), one would expect the trend in

salinity in the Labrador Sea to occur after the drop in the central North Atlantic because it would take time for the lower-salinity water to reach the Labrador Sea via the Irminger Current. Similarly, the magnitudes of the negative anomalies in salinity that are observed in the Labrador Sea are greater than the more gradual decline in the central North Atlantic (Fig. 7). These observations are inconsistent with the mechanism that Labrador Sea anomalies are simply inherited from upstream via a weakened AMOC.

The initial strengthening of the gyre in response to a persistently positive NAO has been shown to be followed in about 10 years by a weakening of the gyre. This appears to result from increased advection of warm water from the subtropical gyre region by a stronger AMOC (Lohmann et al. 2009; Yeager et al. 2012). It is therefore necessary to distinguish between year-to-year variability, such as the negative excursions in salinity in 2008, 2012, and 2015, and longer-term trends. Those trends, possibly corresponding to a weakening or strengthening of the AMOC, will likely dominate only on decadal or longer time scales.

Whether owing to changes in the AMOC or to local forcings, variability in deep convection might affect

salinity in the upper ocean. This would be part of the vertical entrainment term of the salt budget where $w_e \Delta S$ is reduced such that there is an accumulation of meltwater in the summer that stays near the surface and does not get mixed into the deep ocean. Despite anomalous low salinity periods in 2008, 2012, and 2015, it does not appear that there is a lasting effect on density structure within the Labrador Sea. In fact, [Yashayaev and Loder \(2017\)](#) show that since 2012 deep convection has intensified to record depths in the Labrador Sea. This is surprising given the observed variability in surface salinity presented in this study, which suggests that the density structure of the upper ocean has been mainly influenced by the heat removal that occurred during recent positive NAO conditions than it was by the freshening of the upper layers in the Labrador Sea ([Yashayaev and Loder 2017](#)).

[Bersch et al. \(2007\)](#) showed that during the NAO-low period in the mid-1990s, the SPG contracted, causing a northwest shift in the subarctic front that facilitated the pathway of warm and saline waters into the SPG and Nordic seas ([Bersch et al. 2007; Häkkinen and Rhines 2009](#)). This warm and saline anomaly was first detected in the Iceland basin in 1996/97 and then believed to be advected into the SPG reaching the Labrador Sea in 2003/04 ([Bersch et al. 2007](#)). This anomaly has been associated with an average mean salinity increase of more than 0.7 psu in the upper 200 m of the Labrador Sea ([Yashayaev et al. 2015](#)). It is likely that the overall negative trend that is observed in the present study for the Labrador Sea is partly a result of the anomalously high salinity that was advected into the Labrador Sea around the start of the RG dataset.

This study suggests that the overall circulation strength of the SPG plays a major role in establishing the salinity trends that are observed in the western subpolar region and Labrador Sea. [Figure 12](#) shows that changes in upper-20-m salinity in the western SPG are negatively correlated with the intensity of gyre during the months of June to September when the presence of meltwater is expected. However, as noted in [Born et al. \(2016\)](#), on longer time scales stronger gyre circulation might actually increase the westward transport of salt, which should lead to an increase in salinity in the Irminger and Labrador Seas due to increased volume transport. The results presented here suggest that on shorter time scales the relationship between salinity in the western SPG and SPG strength is determined by a wider range of influences than only the advection of salt by basinwide circulation. It should be noted that owing to the relatively short observational record of this study (12 yr), it is not possible to confirm the results of [Born et al. \(2016\)](#). The results here suggest that the surface salinity in the western subpolar

region and Labrador Sea is affected not only by the salinity of the waters flowing from the eastern SPG but also by the interplay between freshwater inputs and the interannual variability of gyre strength. This is particularly important during summer months when sea ice and the Greenland ice sheet are melting. With a stronger SPG, meltwater is transported to the western SPG effectively leading to negative salinity anomalies.

The variability of the SPG strength in turn follows the variability of wind stress curl in the eastern subpolar North Atlantic. This is in accordance with a previous study by [Spall and Pickart \(2003\)](#), who describe the relationship between SPG circulation and wind stress curl east of Greenland. The study shows that the cyclonic circulation of the gyre is driven by seasonally varying wind stress curl and is influenced by the steep topography of the continental slope and weak stratification. In general, the present findings are consistent with a relationship between gyre spinup and wind stress curl, though [Spall and Pickart \(2003\)](#) did not identify the time lag of 6–12 months seen in [Fig. 18d](#). It has also been demonstrated that the seasonal to interannual transport variability of the East Greenland–Irminger Current is consistent with the variability of wind stress curl east of Greenland ([Daniall et al. 2011](#)). However, it is important to note that variability in wind stress is not the only factor in controlling the strength of the SPG. For example, [Häkkinen and Rhines \(2004\)](#) suggest that the weakening of the gyre in the 1990s resulted from changes to local surface buoyancy rather than changes to local wind stress curl. Based on the results of a conceptual four-box model of the western Atlantic subpolar gyre and the Labrador and Irminger Seas, [Born and Stocker \(2014\)](#) quantified the relative impacts of wind and buoyancy forcing and determined that the loss of buoyancy at the surface drives up to 25% of the total circulation of the SPG.

5. Summary and conclusions

Recent trends in mean salinity in the upper 20 m were examined in the North Atlantic for available OA and reanalysis products. Both the complete set from 2005 to 2015 and a subset of OA products from 2004 to 2015 show a general decrease in salinity in the northern North Atlantic, especially in the central North Atlantic and western SPG, including the Labrador Sea. Key differences in the temporal variability of upper salinity occur, such as large negative salinity anomalies in 2008, 2012, and 2015 in the Labrador Sea and western SPG that are not apparent in other regions, such as the central North Atlantic. Thus, the negative trend and interannual variability do not seem to derive from the same processes.

Salinity changes in the SPG are likely governed by multiple processes, and the dominant process affecting salinity can be different from year to year. Nonetheless, it has been clearly demonstrated that widespread freshening of the North Atlantic must result from interaction of increased freshwater fluxes and gyre circulation leading in turn to a concentration of low-salinity waters. Therefore, increased freshwater fluxes and gyre circulation are shown to be important factors in establishing the trend in the western SPG and Labrador Sea. In contrast, atmospheric freshwater fluxes show that the freshening observed from 2004 to 2015 did not result from an $E - P$ imbalance. Because the trend in the western SPG and Labrador Sea region is slightly positive, the cause of the observed salinity trend must be related to changes in ocean processes (e.g., freshwater being advected into the area) and not local changes in air-sea freshwater fluxes. For example, the runoff and subsequent advection of glacial meltwater from Greenland is becoming an important factor influencing surface salinity in the Labrador Sea (Böning et al. 2016; Luo et al. 2016; Yang et al. 2016).

According to previous studies, such as Häkkinen et al. (2011), the circulation strength of the SPG, affected in large part by wind stress curl, plays a major role in establishing the observed salinity trends in the eastern subpolar North Atlantic. Here we also establish a connection between gyre strength and salinity in the western subpolar region and Labrador Sea. Changes in surface salinity in the western SPG are directly correlated with the intensity of the gyre (when considering the period June–October). A stronger SPG is linked to greater wind stress curl over the eastern subpolar North Atlantic, but with an associated time lag of 6–12 months, the cause of which is beyond the scope of the present study.

The circulation strength of the SPG affects accumulation of freshwater in the Labrador Sea. Accounting for the SPG circulation strength is crucial when studying future salinity changes in the upper layers of the subpolar North Atlantic, especially since sources of freshwater from the melting Greenland ice sheet and outflow from the Arctic via the Davis Strait and Fram Strait are expected to increase. Given that Arctic freshwater fluxes have not significantly changed over this study's period (Haine et al. 2015) it is likely not driving the currently observed trends in the Labrador Sea, but the freshwater that has accumulated in the Arctic (Rabe et al. 2014) is anticipated to eventually reach the North Atlantic. Therefore, the stage has been set for enduring declining trends in North Atlantic salinity as a result of Arctic–North Atlantic exchanges.

A continuing decline in surface salinity in the subpolar North Atlantic implies a weakening or halting of deep

convection and meridional overturning circulation (Rahmstorf et al. 2015), although a recent study indicates that to date, Greenland meltwater accumulation has not decreased salinity enough, given historic variability in salinity, to have an appreciable effect on the AMOC (Böning et al. 2016). The increased water column stratification resulting from a decline in surface salinity is also likely to impact vertical mixing of nutrients into the eutrophic zone and primary productivity and carbon export in the subpolar North Atlantic and over the continental shelf of the northwest Atlantic (Greene et al. 2012).

Acknowledgments. JET acknowledges funding from NASA's Goddard Space Flight Center (Award NNX15AN27H). JIG acknowledges support from NASA's Goddard Space Flight Center (Award NNX10AP10G), the Gordon and Betty Moore Foundation (Award GBMF3941), and the Alfred P. Sloan Foundation (Award SLOAN 2014-5-06 DS). Research by ALG was supported by the U.S. Office of Naval Research Global (Award N00014-14-10065). TWNH was supported by NSF Award 118123 and NOAA Award NA15OAR4310172. The authors also thank three reviewers for their helpful comments on this manuscript. Furthermore, this study acknowledges the many datasets that have been made available for public use. The study was made possible by the international Argo program and all the research groups and institutions (AVISO, CLS, CMEMS, CSIO, GPCP, ECCO, ECMWF, IFREMER, IPRC, JAMSTEC, SIO, Mercator Ocean, Met Office Hadley Centre, NOAA/ESRL, and OAFlux) that made their data products publicly available.

REFERENCES

- Adler, R. F., and Coauthors, 2003: The Version-2 Global Precipitation Climatology Project (GPCP) monthly precipitation analysis (1979–present). *J. Hydrometeor.*, **4**, 1147–1167, [https://doi.org/10.1175/1525-7541\(2003\)004<1147:TVGCP>2.0.CO;2](https://doi.org/10.1175/1525-7541(2003)004<1147:TVGCP>2.0.CO;2).
- Bamber, J., M. van den Broeke, J. Ettema, J. Lenaerts, and E. Rignot, 2012: Recent large increases in freshwater fluxes from Greenland into the North Atlantic. *Geophys. Res. Lett.*, **39**, L19501, <https://doi.org/10.1029/2012GL052552>.
- Belkin, I. M., 2004: Propagation of the “Great Salinity Anomaly” of the 1990s around the northern North Atlantic. *Geophys. Res. Lett.*, **31**, L08306, <https://doi.org/10.1029/2003GL019334>.
- , S. Levitus, J. Antonov, and S.-A. Malmberg, 1998: “Great Salinity Anomalies” in the North Atlantic. *Prog. Oceanogr.*, **41**, 1–68, [https://doi.org/10.1016/S0079-6611\(98\)00015-9](https://doi.org/10.1016/S0079-6611(98)00015-9).
- Bersch, M., I. Yashayaev, and K. P. Koltermann, 2007: Recent changes of the thermohaline circulation in the subpolar North Atlantic. *Ocean Dyn.*, **57**, 223–235, <https://doi.org/10.1007/s10236-007-0104-7>.
- Bisagni, J. J., A. Gangopadhyay, and A. Sanchez-Franks, 2017: Secular change and inter-annual variability of the Gulf Stream

- position, 1993–2013, 70°–55°W. *Deep-Sea Res. I*, **125**, 1–10, <https://doi.org/10.1016/j.dsr.2017.04.001>.
- Böning, C. W., E. Behrens, A. Biastoch, K. Getzlaff, and J. L. Bamber, 2016: Emerging impact of Greenland meltwater on deepwater formation in the North Atlantic Ocean. *Nat. Geosci.*, **9**, 523–527, <https://doi.org/10.1038/ngeo2740>.
- Born, A., and T. F. Stocker, 2014: Two stable equilibria of the Atlantic subpolar gyre. *J. Phys. Oceanogr.*, **44**, 246–264, <https://doi.org/10.1175/JPO-D-13-073.1>.
- , —, and A. B. Sandø, 2016: Transport of salt and freshwater in the Atlantic Subpolar Gyre. *Ocean Dyn.*, **66**, 1051–1064, <https://doi.org/10.1007/s10236-016-0970-y>.
- Boyer, T., S. Levitus, J. Antonov, R. Locarnini, A. Mishonov, H. Garcia, and S. A. Josey, 2007: Changes in freshwater content in the North Atlantic Ocean 1955–2006. *Geophys. Res. Lett.*, **34**, L16603, <https://doi.org/10.1029/2007GL030126>.
- Buckley, M. W., and J. Marshall, 2016: Observations, inferences, and mechanisms of the Atlantic meridional overturning circulation: A review. *Rev. Geophys.*, **54**, 5–63, <https://doi.org/10.1002/2015RG000493>.
- Cabanes, C., and Coauthors, 2013: The CORA dataset: Validation and diagnostics of in-situ ocean temperature and salinity measurements. *Ocean Sci.*, **9**, 1–18, <https://doi.org/10.5194/os-9-1-2013>.
- Chaudhuri, A. H., R. M. Ponte, G. Forget, and P. Heimbach, 2013: A comparison of atmospheric reanalysis surface products over the ocean and implications for uncertainties in AirSea boundary forcing. *J. Climate*, **26**, 153–170, <https://doi.org/10.1175/JCLI-D-12-00090.1>.
- Comiso, J. C., C. L. Parkinson, R. Gersten, and L. Stock, 2008: Accelerated decline in the Arctic sea ice cover. *Geophys. Res. Lett.*, **35**, L16603, <https://doi.org/10.1029/2007GL031972>.
- Curry, R., and C. Mauritzen, 2005: Dilution of the northern North Atlantic Ocean in recent decades. *Science*, **308**, 1772–1774, <https://doi.org/10.1126/science.1109477>.
- , B. Dickson, and I. Yashayaev, 2003: A change in the freshwater balance of the Atlantic Ocean over the past four decades. *Nature*, **426**, 826–829, <https://doi.org/10.1038/nature02206>.
- Daniault, N., H. Mercier, and P. Lherminier, 2011: The 1992–2009 transport variability of the east Greenland-Irminger Current at 60°N. *Geophys. Res. Lett.*, **38**, L07601, <https://doi.org/10.1029/2011GL046863>.
- Dee, D. P., and Coauthors, 2011: The ERA-Interim reanalysis: Configuration and performance of the data assimilation system. *Quart. J. Roy. Meteor. Soc.*, **137**, 553–597, <https://doi.org/10.1002/qj.828>.
- Déry, S. J., M. A. Hernández-Henríquez, J. E. Burford, and E. F. Wood, 2009: Observational evidence of an intensifying hydrological cycle in northern Canada. *Geophys. Res. Lett.*, **36**, L13402, <https://doi.org/10.1029/2009GL038852>.
- Dickson, B., I. Yashayaev, J. Meincke, B. Turrell, S. R. Dye, and J. Holfort, 2002: Rapid freshening of the deep North Atlantic Ocean over the past four decades. *Nature*, **416**, 832–837, <https://doi.org/10.1038/416832a>.
- Dickson, R. R., J. Meincke, S.-A. Malmberg, and A. J. Lee, 1988: The “Great Salinity Anomaly” in the northern North Atlantic 1968–1982. *Prog. Oceanogr.*, **20**, 103–151, [https://doi.org/10.1016/0079-6611\(88\)90049-3](https://doi.org/10.1016/0079-6611(88)90049-3).
- Doyle, J. D., and M. A. Shapiro, 1999: Flow response to large-scale topography: The Greenland tip jet. *Tellus*, **51A**, 728–748, <https://doi.org/10.3402/tellusa.v51i5.14471>.
- Durack, P. J., S. E. Wijffels, and R. J. Matear, 2012: Ocean salinities reveal strong global water cycle intensification during 1950 to 2000. *Science*, **336**, 455–458, <https://doi.org/10.1126/science.1212222>.
- Dyurgerov, M., A. Bring, and G. Destouni, 2010: Integrated assessment of changes in freshwater inflow to the Arctic Ocean. *J. Geophys. Res.*, **115**, D12116, <https://doi.org/10.1029/2009JD013060>.
- Eden, C., and T. Jung, 2001: North Atlantic interdecadal variability: Oceanic response to the North Atlantic Oscillation (1865–1997). *J. Climate*, **14**, 676–691, [https://doi.org/10.1175/1520-0442\(2001\)014<0676:NAIVOR>2.0.CO;2](https://doi.org/10.1175/1520-0442(2001)014<0676:NAIVOR>2.0.CO;2).
- , and J. Willebrand, 2001: Mechanism of interannual to decadal variability of the North Atlantic circulation. *J. Climate*, **14**, 2266–2280, [https://doi.org/10.1175/1520-0442\(2001\)014<2266:MOITDV>2.0.CO;2](https://doi.org/10.1175/1520-0442(2001)014<2266:MOITDV>2.0.CO;2).
- Forget, G., J.-M. Campin, P. Heimbach, C. N. Hill, R. M. Ponte, and C. Wunsch, 2015: ECCO version 4: An integrated framework for non-linear inverse modeling and global ocean state estimation. *Geosci. Model Dev.*, **8**, 3071–3104, <https://doi.org/10.5194/gmd-8-3071-2015>.
- Fratantoni, P. S., and R. S. Pickart, 2003: Variability of the shelf break jet in the Middle Atlantic Bight: Internally or externally forced? *J. Geophys. Res.*, **108**, 3166, <https://doi.org/10.1029/2002JC001326>.
- Gaillard, F., T. Reynaud, V. Thierry, N. Kolodziejczyk, and K. von Schuckmann, 2016: In situ-based reanalysis of the global ocean temperature and salinity with ISAS: Variability of the heat content and steric height. *J. Climate*, **29**, 1305–1323, <https://doi.org/10.1175/JCLI-D-15-0028.1>.
- Gawarkiewicz, G. G., R. E. Todd, A. J. Plueddemann, M. Andres, and J. P. Manning, 2012: Direct interaction between the Gulf Stream and the shelfbreak south of New England. *Sci. Rep.*, **2**, 553, <https://doi.org/10.1038/srep00553>.
- Gelderloos, R., F. Straneo, and C. A. Katsman, 2012: Mechanisms behind the temporary shutdown of deep convection in the Labrador Sea: Lessons from the Great Salinity Anomaly years 1968–71. *J. Climate*, **25**, 6743–6755, <https://doi.org/10.1175/JCLI-D-11-00549.1>.
- Good, S. A., M. J. Martin, and N. A. Rayner, 2013: EN4: Quality controlled ocean temperature and salinity profiles and monthly objective analyses with uncertainty estimates. *J. Geophys. Res. Oceans*, **118**, 6704–6716, <https://doi.org/10.1002/2013JC009067>.
- Greene, C. H., and Coauthors, 2012: Recent Arctic climate change and its remote forcing of northwest Atlantic shelf ecosystems. *Oceanography*, **25** (3), 208–213, <https://doi.org/10.5670/oceanog.2012.64>.
- Guinehut, S., A. L. Dhomps, G. Larnicol, and P.-Y. Le Traon, 2012: High resolution 3-D temperature and salinity fields derived from in situ and satellite observations. *Ocean Sci.*, **8**, 845–857, <https://doi.org/10.5194/os-8-845-2012>.
- Haine, T. W. N., 2016: Vagaries of Atlantic overturning. *Nat. Geosci.*, **9**, 479–480, <https://doi.org/10.1038/ngeo2748>.
- , and Coauthors, 2015: Arctic freshwater export: Status, mechanisms, and prospects. *Global Planet. Change*, **125**, 13–35, <https://doi.org/10.1016/j.gloplacha.2014.11.013>.
- Häkkinen, S., 2002: Freshening of the Labrador Sea surface waters in the 1990s: Another Great Salinity Anomaly? *Geophys. Res. Lett.*, **29**, 2232, <https://doi.org/10.1029/2002GL015243>.
- , and P. B. Rhines, 2004: Decline of subpolar North Atlantic circulation during the 1990s. *Science*, **304**, 555–559, <https://doi.org/10.1126/science.1094917>.
- , and —, 2009: Shifting surface currents in the northern North Atlantic Ocean. *J. Geophys. Res.*, **114**, C04005, <https://doi.org/10.1029/2008JC004883>.

- , —, and D. L. Worthen, 2011: Warm and saline events embedded in the meridional circulation of the northern North Atlantic. *J. Geophys. Res.*, **116**, C03006, <https://doi.org/10.1029/2010JC006275>.
- Hanna, E., and Coauthors, 2014: Atmospheric and oceanic climate forcing of the exceptional Greenland ice sheet surface melt in summer 2012. *Int. J. Climatol.*, **34**, 1022–1037, <https://doi.org/10.1002/joc.3743>.
- Hosoda, S., T. Ohira, and T. Nakamura, 2008: A monthly mean dataset of global oceanic temperature and salinity derived from Argo float observations. *JAMSTEC Rep. Res. Dev.*, **8**, 47–59, <https://doi.org/10.5918/jamstecr.8.47>.
- Houssais, M.-N., C. Herbaut, P. Schlichtholz, and C. Rousset, 2007: Arctic salinity anomalies and their link to the North Atlantic during a positive phase of the Arctic Oscillation. *Prog. Oceanogr.*, **73**, 160–189, <https://doi.org/10.1016/j.pocean.2007.02.005>.
- Hurrell, J. W., and C. Deser, 2009: North Atlantic climate variability: The role of the North Atlantic Oscillation. *J. Mar. Syst.*, **78**, 28–41, <https://doi.org/10.1016/j.jmarsys.2008.11.026>.
- Jackson, L. C., K. A. Peterson, C. D. Roberts, and R. A. Wood, 2016: Recent slowing of Atlantic overturning circulation as a recovery from earlier strengthening. *Nat. Geosci.*, **9**, 518–522, <https://doi.org/10.1038/ngeo2715>.
- Johnson, G. C., and J. M. Lyman, 2016: Sea surface salinity [in “State of the Climate in 2015”]. *Bull. Amer. Meteor. Soc.*, **97** (8), S71–S72.
- Kattsov, V. M., and J. E. Walsh, 2000: Twentieth-century trends of Arctic precipitation from observational data and a climate model simulation. *J. Climate*, **13**, 1362–1370, [https://doi.org/10.1175/1520-0442\(2000\)013<1362:TCTOAP>2.0.CO;2](https://doi.org/10.1175/1520-0442(2000)013<1362:TCTOAP>2.0.CO;2).
- Lazier, J. R. N., 1980: Oceanographic conditions at Ocean Weather Ship *Bravo*, 1964–1974. *Atmos.–Ocean*, **18**, 227–238, <https://doi.org/10.1080/07055900.1980.9649089>.
- Li, H., F. Xu, W. Zhou, D. Wang, J. S. Wright, Z. Liu, and Y. Lin, 2017: Development of a global gridded Argo data set with Barnes successive corrections. *J. Geophys. Res. Oceans*, **122**, 866–889, <https://doi.org/10.1002/2016JC012285>.
- Li, Y., P. S. Frantoni, C. Chen, J. A. Hare, Y. Sun, R. C. Beardsley, and R. Ji, 2015: Spatio-temporal patterns of stratification on the northwest Atlantic shelf. *Prog. Oceanogr.*, **134**, 123–137, <https://doi.org/10.1016/j.pocean.2015.01.003>.
- Linder, C. A., and G. Gawarkiewicz, 1998: A climatology of the shelfbreak front in the Middle Atlantic Bight. *J. Geophys. Res.*, **103**, 18405–18423, <https://doi.org/10.1029/98JC01438>.
- Lohmann, K., H. Drange, and M. Bentsen, 2009: Response of the North Atlantic subpolar gyre to persistent North Atlantic Oscillation like forcing. *Climate Dyn.*, **32**, 273–285, <https://doi.org/10.1007/s00382-008-0467-6>.
- Luo, H., R. M. Castelao, A. K. Rennermalm, M. Tedesco, A. Bracco, P. L. Yager, and T. L. Mote, 2016: Oceanic transport of surface meltwater from the southern Greenland ice sheet. *Nat. Geosci.*, **9**, 528–532, <https://doi.org/10.1038/ngeo2708>.
- Marshall, J., and F. Schott, 1999: Open-ocean convection: Observations, theory, and models. *Rev. Geophys.*, **37**, 1–64, <https://doi.org/10.1029/98RG02739>.
- Mauritzen, C., A. Melsom, and R. T. Sutton, 2012: Importance of density-compensated temperature change for deep North Atlantic Ocean heat uptake. *Nat. Geosci.*, **5**, 905–910, <https://doi.org/10.1038/ngeo1639>.
- McDougall, T. J., and P. M. Barker, 2011: Getting started with TEOS-10 and the Gibbs Seawater (GSW) oceanographic toolbox. SCOR/IAPSO Tech. Rep., 28 pp., http://www.teos-10.org/pubs/Getting_Started.pdf.
- Nghiem, S. V., and Coauthors, 2012: The extreme melt across the Greenland ice sheet in 2012. *Geophys. Res. Lett.*, **39**, L20502, <https://doi.org/10.1029/2012GL053611>.
- Parkinson, C. L., and J. C. Comiso, 2013: On the 2012 record low Arctic sea ice cover: Combined impact of preconditioning and an August storm. *Geophys. Res. Lett.*, **40**, 1356–1361, <https://doi.org/10.1002/grl.50349>.
- Peterson, B. J., R. M. Holmes, J. W. McClelland, C. J. Vörösmarty, R. B. Lammers, A. I. Shiklomanov, I. A. Shiklomanov, and S. Rahmstorf, 2002: Increasing river discharge to the Arctic Ocean. *Science*, **298**, 2171–2173, <https://doi.org/10.1126/science.1077445>.
- , J. McClelland, R. Curry, R. M. Holmes, J. E. Walsh, and K. Aagaard, 2006: Trajectory shifts in the Arctic and subarctic freshwater cycle. *Science*, **313**, 1061–1066, <https://doi.org/10.1126/science.1122593>.
- Proshutinsky, A., and Coauthors, 2009: Beaufort Gyre freshwater reservoir: State and variability from observations. *J. Geophys. Res.*, **114**, C00A10, <https://doi.org/10.1029/2008JC005104>.
- Rabe, B., and Coauthors, 2014: Arctic Ocean basin liquid freshwater storage trend 1992–2012. *Geophys. Res. Lett.*, **41**, 961–968, <https://doi.org/10.1002/2013GL058121>.
- Rahmstorf, S., J. E. Box, G. Feulner, M. E. Mann, A. Robinson, S. Rutherford, and E. J. Schaffernicht, 2015: Exceptional twentieth-century slowdown in Atlantic Ocean overturning circulation. *Nat. Climate Change*, **5**, 475–480, <https://doi.org/10.1038/nclimate2554>.
- Ren, L., K. Speer, and E. P. Chassignet, 2011: The mixed layer salinity budget and sea ice in the Southern Ocean. *J. Geophys. Res.*, **116**, C08031, <https://doi.org/10.1029/2010JC006634>.
- Riser, S. C., and Coauthors, 2016: Fifteen years of ocean observations with the global Argo array. *Nat. Climate Change*, **6**, 145–153, <https://doi.org/10.1038/nclimate2872>.
- Robson, J., P. Ortega, and R. Sutton, 2016: A reversal of climatic trends in the North Atlantic since 2005. *Nat. Geosci.*, **9**, 513–517, <https://doi.org/10.1038/ngeo2727>.
- Roemmich, D., and J. Gilson, 2009: The 2004–2008 mean and annual cycle of temperature, salinity, and steric height in the global ocean from the Argo Program. *Prog. Oceanogr.*, **82**, 81–100, <https://doi.org/10.1016/j.pocean.2009.03.004>.
- Roessler, A., M. Rhein, D. Kieke, and C. Mertens, 2015: Long-term observations of North Atlantic Current transport at the gateway between western and eastern Atlantic. *J. Geophys. Res. Oceans*, **120**, 4003–4027, <https://doi.org/10.1002/2014JC010662>.
- Sarafanov, A., and Coauthors, 2012: Mean full-depth summer circulation and transports at the northern periphery of the Atlantic Ocean in the 2000s. *J. Geophys. Res.*, **117**, C01014, <https://doi.org/10.1029/2011JC007572>.
- Schlundt, M., P. Brandt, M. Dengler, R. Hummels, T. Fischer, K. Bumke, G. Krahmann, and J. Karstensen, 2014: Mixed layer heat and salinity budgets during the onset of the 2011 Atlantic cold tongue. *J. Geophys. Res. Oceans*, **119**, 7882–7910, <https://doi.org/10.1002/2014JC010021>.
- Spall, M. A., and R. S. Pickart, 2003: Wind-driven recirculations and exchange in the Labrador and Irminger Seas. *J. Phys. Oceanogr.*, **33**, 1829–1845, <https://doi.org/10.1175/2384.1>.
- Stewart, K. D., and T. W. N. Haine, 2013: Wind-driven Arctic freshwater anomalies. *Geophys. Res. Lett.*, **40**, 6196–6201, <https://doi.org/10.1002/2013GL058247>.
- Straneo, F., 2006: Heat and freshwater transport through the central Labrador Sea. *J. Phys. Oceanogr.*, **36**, 606–628, <https://doi.org/10.1175/JPO2875.1>.
- Toole, J. M., R. A. Krishfield, M.-L. Timmermans, and A. Proshutinsky, 2011: The Ice-Tethered Profiler: Argo of the

- Arctic. *Oceanography*, **24** (3), 126–135, <https://doi.org/10.5670/oceanog.2011.64>.
- Våge, K., and Coauthors, 2011: The Irminger Gyre: Circulation, convection, and interannual variability. *Deep-Sea Res. I*, **58**, 590–614, <https://doi.org/10.1016/j.dsr.2011.03.001>.
- von Schuckmann, K., and Coauthors, 2016: The Copernicus marine environment monitoring service ocean state report. *J. Oper. Oceanogr.*, **9** (Suppl.), S235–S320, <https://doi.org/10.1080/1755876X.2016.1273446>.
- Yang, Q., T. H. Dixon, P. G. Myers, J. Bonin, D. Chambers, and M. R. van den Broeke, 2016: Recent increases in Arctic freshwater flux affects Labrador Sea convection and Atlantic overturning circulation. *Nat. Commun.*, **7**, 10525, <https://doi.org/10.1038/ncomms10525>.
- Yashayaev, I., and J. W. Loder, 2017: Further intensification of deep convection in the Labrador Sea in 2016. *Geophys. Res. Lett.*, **44**, 1429–1438, <https://doi.org/10.1002/2016GL071668>.
- , D. Seidov, and E. Demirov, 2015: A new collective view of oceanography of the Arctic and North Atlantic basins. *Prog. Oceanogr.*, **132**, 1–21, <https://doi.org/10.1016/j.pocean.2014.12.012>.
- Yeager, S., A. Karspeck, G. Danabasoglu, J. Tribbia, and H. Teng, 2012: A decadal prediction case study: Late twentieth-century North Atlantic Ocean heat content. *J. Climate*, **25**, 5173–5189, <https://doi.org/10.1175/JCLI-D-11-00595.1>.
- Yelland, M., and P. K. Taylor, 1996: Wind stress measurements from the open ocean. *J. Phys. Oceanogr.*, **26**, 541–558, [https://doi.org/10.1175/1520-0485\(1996\)026<0541:WSMFTO>2.0.CO;2](https://doi.org/10.1175/1520-0485(1996)026<0541:WSMFTO>2.0.CO;2).
- Yu, L., 2007: Global variations in oceanic evaporation (1958–2005): The role of the changing wind speed. *J. Climate*, **20**, 5376–5390, <https://doi.org/10.1175/2007JCLI1714.1>.
- , 2011: A global relationship between the ocean water cycle and near-surface salinity. *J. Geophys. Res.*, **116**, C10025, <https://doi.org/10.1029/2010JC006937>.